Molecules and heterostructures at TiO2 surface: the cases of H2O, CO2, and organic and inorganic sensitizers

Molecules and heterostructures at TiO_2 surface: the cases of H_2O, CO_2, and organic and inorganic sensitizers

Lorenzo Mino, Federico Cesano, Domenica Scarano, Giuseppe Spoto, Gianmario Martra*

Department of Chemistry and Interdepartmental Centre "Nanostructured Interfaces and Surfaces – NIS", University of Torino, via Giuria 7, 10125 Torino, Italy

* Correponding author; E-mail: gianmario.martra@unito.it

Abstract

TiO_2-based (nano)materials are widely exploited in systems and devices of actual technological interest, because of their outstanding physical and chemical properties, including chemical stability, long durability, non-toxicity abundance and low cost. For this they are considered ideal for many practical applications including energy-related devices, photocatalysis, but are known to have some limitations. To improve their performance and then to find more efficient materials in the energy and environmental remediation fields, at first the investigation of the surface/interface properties at the molecular scale is required. In this contribution, a critical review of advances in the field of the TiO_2 surface chemistry, highlighting the role of interactions at the molecular level, grafting and assembling/fabrication of suitable heterostructures, is reported. A few case studies, from the H_2O, CO_2 and acetylene interactions until to the grafting of organic/inorganic systems (graphene, MoS_2) at the TiO_2 surface, are highlighted. The discussed case studies are argued from their principles to the technological relevance.

Keywords: TiO_2 photocatalysis; H_2O, CO_2 and C_2H_2 adsorption; graphene/ and MoS_2/TiO_2 hybrids; surface heterostrucures; IR spectroscopy; STM and AFM; HTREM; electronic spectroscopy; quantum modelling.

Contents:

1. Preliminary remarks: motivation and structure of this review

Particles and nanoparticles resulting from the combination of titanium, the second transition element more common in Earth's crust after iron, with oxygen to form TiO_2, mainly in the anatase and rutile phases, are used in a wide array of products, devices and technologies. As reported by the Titanium Dioxide Manufacturers Associations (TDMA, https://tdma.info), gathering since 1974 the major producers of this material in Europe, the commercial and research area representing the "first coordination sphere" of the authors of this review, application for TiO_2 across the EU, as well as across the globe, include paints, papers, pharmaceuticals, sunscreen and food (where it is listed as colourant E171). As a photocatalyst, titanium dioxide can be added to paints, cements, windows and tiles in order to decompose environmental pollutants, and as a white pigment (in this case called titanium white, Pigment White 6 or CI 77891), TiO_2 is one of the most important raw materials for paints and coatings. Moreover, the range of innovative uses for TiO_2 keeps on increasing. In recent years, for example, it has been used in the manufacture of cheap and efficient solar cells and building facades that can neutralise air pollution.

In almost all these applications, the performances of these particles and nanoparticles are ruled, in a large extent, by their surface properties, or, more precisely, by the interaction of their surface with molecules and/or heterostructures. On the basis of our expertise, here we propose a mini-review on four topics where we were able to contribute in the last years, namely TiO_2 nanoparticles in interaction with water, CO_2, organic and inorganic heterostructures intended as sensitizers towards the response to visible light. Thus, the first section is a summary of the technological relevance of these topics, followed by sections devoted to scientific insights on each of the four surface/interfacial interactions considered. A particular attention has been devoted to results provided by IR spectroscopy in controlled conditions, of course augmented by other relevant methods as tip-based microscopies (STM, AFM), high-resolution transmission electron microscopy, electronic spectroscopy, and quantum modelling.

2. Introduction: technological relevance of the TiO_2-based systems considered

2.1 Water at anatase TiO_2 surfaces

The interaction of H_2O molecules with anatase TiO_2 surface is a cornerstone of the technological exploitation of this semiconductor oxide, since Fujishima and Honda discovered the possibility to attain the electrochemical photolysis of water on a TiO_2-based electrode [1]. Up today, the research on this fundamental topic for the sustainable energy production flourished, and a variety of factors with a possible beneficial impact on the effectiveness of this process have been investigated. As far as the tuning of photoactive materials is concerned, the surface functionalization with metals, and in

particular noble metals like Au and Pt is widely recognized as an effective strategy to promote water splitting, even under solar light irradiation [2]. In some case, the functionalization with Pt particles was coupled with a pre-modification of the TiO_2 support, like titania thin films treated with HF solution, which in their bare form were found to exhibit a remarkable enhancement of the photocatalytic activity for H_2 evolution from a methanol aqueous solution, as compared with the untreated TiO_2 [3]. Still on the effect of Pt as co-catalyst, the results obtained by XPS and XRD measurements of Pt-loaded TiO_2 the as a function of the calcination temperature as well as the photocatalytic decomposition reactions of H_2O clearly indicate that controlling the oxidation state of Pt as well as the amount of loaded Pt species are both important factors in the design of water-splitting photocatalysts having high efficiency and stoichiometry [4].

Also mixed oxides were found to act as noble-metal free alternative to the previous systems, with significant improvements in hydrogen production with respect to bare titania, for instance using TiO_2-ZnO [5] and TiO_2-SiO_2 [6] photocatalysts. Also, for these materials the tuning of the preparation conditions has an important impact on their performances. For instance, it was shown that TiO_2-SiO_2 prepared with acetic acid as a chelating agent in a sol-gel with relatively high specific surface area and high photocurrent density were found to have low charge transfer resistance, as well as a wide space charge region, which might result in the superior photocatalytic water decomposition for H_2 production [7].

The other pillar of the chemical exploitation of molecular events occurring in aqueous media at the surface of photostimulated TiO_2- materials are the processes intended to the improvement of the quality of water. The targets are the abatement of both chemical pollutants, like dyes [8, 9], haloderivatives [10, 11], aromatics [12], and biological pollutants, like pathogenic micro-organisms [13].

An important different output of interfacial water-TiO_2 events is the arising of superhydrophilicity of TiO_2 thin films by exposure to UV light [14]. Since the first findings [15], this phenomenon was recognized to have a relevant technological impact for the fabrication of photofunctional materials for self-cleaning, antifogging, antibacterial, and stain-proofing agents ([16, 17] and references therein). Most part of the subsequent applicative efforts has been focused on the induction of such photoinduced superhydrophilicity under visible light irradiation [14].

2.2 Carbon dioxide at anatase TiO_2 surfaces

The interaction and photoreactivity of CO_2 with TiO_2 have been the topic of several studies, both experimental and computational, in the last years. There is a twofold motivation in this kind of investigations: (i) CO_2 is one of the main final products in the photocatalytic degradation of organic

pollutants [18]; (ii) photocatalytic conversion of CO_2 to solar fuels using TiO_2 [19]. The latter point is becoming particularly relevant owing to the increasing concern for the high level of anthropogenic CO_2 emissions and their consequences on the global warming and climate change. In this context, CO_2 valorization by photocatalytic conversion to valuable chemicals could be a promising way to reduce its concentration in the atmosphere [20]. Since CO_2, being the most oxidized state of carbon, is a very stable molecule, its one-electron reduction is extremely endergonic (−1.9 V vs. SHE) [21] and therefore unsuitable for practical applications. However, proton-coupled multi-electron reduction processes of CO_2 are less thermodynamically demanding and, thus, appear more promising. Transition metal complexes show excellent photocatalytic activity in this kind of reactions, but are often based on expensive elements (e.g. Ru, Os, Re) [22]. Conversely, photocatalytic systems based on semiconductor nanoparticles (e.g. TiO_2, ZnO, CdS, WO_3, ZrO_2, ZnS) [21] could represent a cheaper alternative. In particular, TiO_2-based systems are attracting increasing interest [19] and a deeper understanding at the molecular level of the processes occurring when CO_2 is interacting with the most common TiO_2 crystalline phases (i.e. anatase and rutile) could help the development of photocatalysts with improved performance.

2.3 Heterostructures at TiO_2 surface as organic and inorganic sensitizers

In recent years many efforts have been devoted to exploring suitable materials for environmental and inexpensive applications, including the developing of clean energy processes (i.e. energy conversion) and energy storage technologies (i.e. batteries and capacitors) [23].

In particular, among the photoactive materials, considerable efforts were mostly dedicated to exploring surface chemistry of TiO_2 polytypes, [24-28],[29-31], including surface functionalization and grafting of heterostructures, by adopting commonly a multi-technique approach, which helps to correlate morphology, structure with the peculiar properties of the obtained materials [32-36]. Specifically concerning TiO_2 we mention those strategies aiming (i) to extend the TiO_2 light absorption threshold from the UV to the Vis-NIR region and (ii) to prolong the life of the excitons created under irradiation by retarding the electron/hole recombination.

As to strategy (i) doping with metal [37-40] and non-metals [41-43] has been attempted, as well as surface modification by anchoring dye molecules [44-46], quantum dots [36, 47], metal nanoparticles [36, 47-50] or also halides species [29].

Among the many contributions, a case study of anatase TiO_2 surface functionalization was provided by Yang et al. [29]. The authors showed that, when anatase TiO_2 crystals, which are mostly dominated by the thermodynamically stable {101} facets (> 94%), rather than the much reactive {001} ones, react with hydrofluoric acid, the faces relative stability is reversed. In fact, F-terminated TiO_2 surfaces

exhibit a prevalence (47%) of {001} most reactive faces, being HF a morphology controlling agent. Conversely, about 98.7% of {101} facets can be reached with other developed procedures based on HF/alcohol mixtures [51].

As to strategy (ii) great interest has received the preparation of organic/inorganic hybrid materials where TiO_2 is deposited onto or covered with CN (carbon nitride) films [52,53], "common" carbonaceous structures like amorphous or graphitic carbon [54-56], or more "exotic" carbon allotropes like fullerenes, CNTs (Carbon Nano Tubes) and above all graphene [57-61] together with graphene-like materials [62].

The improved photocatalytic activity usually observed for the hybrid materials with respect to the pure oxide is mainly due to the high affinity of the above carbon-based phases for negative charges which allows them to sink across the interface the e^- promoted in the TiO_2 valence band under irradiation. This can open new more favourable channels in the dispatching of the catalytic activity, as well as hindering a detrimental fast e^-/h^+ (electron/hole) recombination [63].

As for the investigation of TiO_2 covered by carbonaceous structures, a section of this review will be devoted to the discussion of the acetylene/TiO_2 interaction, being considered the basis of a complex, but versatile, surface chemistry which can be addressed to the growth under mild conditions (like low temperature and low C_2H_2 pressure) and directly on the TiO_2 surface of a variety of meaningful products. These range from benzene and other small aromatic molecules, to strongly adsorbed coloured oligomeric chains (*i.e.* possible candidates as dyes for the absorption of the Vis-NIR frequencies) up to graphene-like patches, or even continuous graphene layers, uniformly covering the oxide surface (*i.e.* organic surface structures, possibly acting as stabilizers of the TiO_2 photo-charges).

As part of the more general grafting of heterostructures at the surface of TiO_2 polytypes, 2D layered materials such as MoS_2 and other group 6 transition metal dichalcogenides (TMDs) are known to be also effective photosensitizers to TiO_2 surface, thus highlighting their potential in photoelectrochemical applications [64-76]. Due to the strong anisotropy of the TMDs structures, individual monolayers *via* cleavage along the weakly bonded van der Waals planes can be isolated, which gives rise to unique properties with respect to their 3D counterpart [64, 77-80]. Among TMDs, MoS_2, owing to its absorption in the UV−visible range, has attracted increasing interest as a promising material, also for its abundance, low cost, high activity, chemical stability, ability to modify the band gap from an indirect semiconductor (1.3 eV) to a direct semiconductor (1.9 eV), moving from the bulk to ultrathin and nanosized structures [23]. Notice for instance, the high charge carrier separation together with considerable migration efficiencies, the wide light harvesting range, when used as anode materials for rechargeable batteries and enhanced solar hydrogen generation [81-85]. Hence, due to the favourable optical properties of MoS_2, that is, excitonic absorption bands in the visible and the

efficient interfacial charge-transfer region between MoS_2 and TiO_2 based materials, MoS_2 was considered of great interest to perform MoS_2/TiO_2 hybrid composites, made by TiO_2 sensitized with MoS_2, which causes to increase the visible light absorption ability of TiO_2-based systems [65, 86].
However, coming back briefly to the past, MoS_2-based TiO_2 materials, obtained from H_2S sulfidation of TiO_2 supported MoO_3 were mainly used as composite coatings for low-friction and wear-resistant properties [87], for catalytic reduction of N_2O with H_2 [88] or for methanol photo-oxidation [89], then in the '80s for hydrodesulfurization and hydrogenation reactions [90, 91]. It wasn't until the 1990s that the first comprehensive investigations on morphology and structure (i.e. stacking order and defects) of single or few-layered thick MoS_2 grafted on several supports (SiO_2, Al_2O_3, TiO_2 and ZrO_2), were provided by Pratt et al. [92]. Since that, the role played by the MoS_2/support interaction, i.e. interface regions, became relevant also for the discovery of 2D materials (i.e. graphene, other transition metal dichalcogenides) and their heterostructures.
Along these themes, a section of this review will be devoted to a brief discussion of a few case studies of MoS_2-based TiO_2 heterostructures, being the reader referred to the extensive literature published elsewhere.

3. Investigations at molecular level

3.1 Water at TiO_2 anatase surfaces

Independently on the type of technological exploitation, all applications involving water/TiO_2 systems gained a fundamental benefit from the knowledge-based approach targeting the elucidation of what is actually occurring when H_2O molecules interact with TiO_2 surfaces. Among the quite large number of complementary techniques useful for the investigation of the interaction of H_2O molecules with TiO_2 surfaces, (e.g. volumetry, microgravimetry, adsorption calorimetry, XPS, HREELS, SFG-VS, IR, tip-based scanning microscopies), it can be of interest to focus on the results provided by two of them. They are scanning tunneling microscopy (STM), because of its fascinating output consisting in the possibility to "see" molecules on single crystals, and FT-IR spectroscopy in controlled atmosphere, for the easiness of application to the study of the results of both dissociative and molecular adsorption of water on TiO_2 nanoparticles, i.e. surface hydroxylation and hydration, respectively.

3.1.1 Water on TiO_2 anatase (101) single crystal: imaging of H_2O molecular adsorption via STM

For TiO_2 anatase, most of these studies have been carried out on (101) single crystals, being this surface the most stable one for this titania phase. STM imaging of adsorbed H_2O molecules was a way to proof that water adsorbs non-dissociatively on the anatase (101) surface [93, 94]. Its O atom binds to a 5-fold coordinated surface Ti atom, while the H atoms form hydrogen bonds with the two

neighboring surface 2-fold O atoms ([93], also see Fig. 1d). The calculated adsorption energy of H_2O is 730 meV [93] consistent with temperature programmed desorption spectra, which show a broad water desorption peak centred at ~250 K [94]. Noteworthy, the appearance of adsorbed molecules depends on experimental conditions, like tip condition [95]. As an example, Fig. 1a and b show the anatase (101) surface with a small coverage of water. The arrows point out single molecules. As clearly seen in the insets these appear as either bright, extended features, or as three consecutive, bright–dark–bright spots. The molecules' appearance in Fig. 1a is typical for clean, metallic tips; in this case the appearance does not depend strongly on the sample bias. The contrast in Fig. 1b was frequently encountered for sample temperatures in the range from 180 to 220 K; at conditions where thermal diffusion of water molecules across the surface becomes facile [93]. Possibly, a H_2O molecule (or a fragment thereof) hops to the STM tip, resulting in this specific contrast.

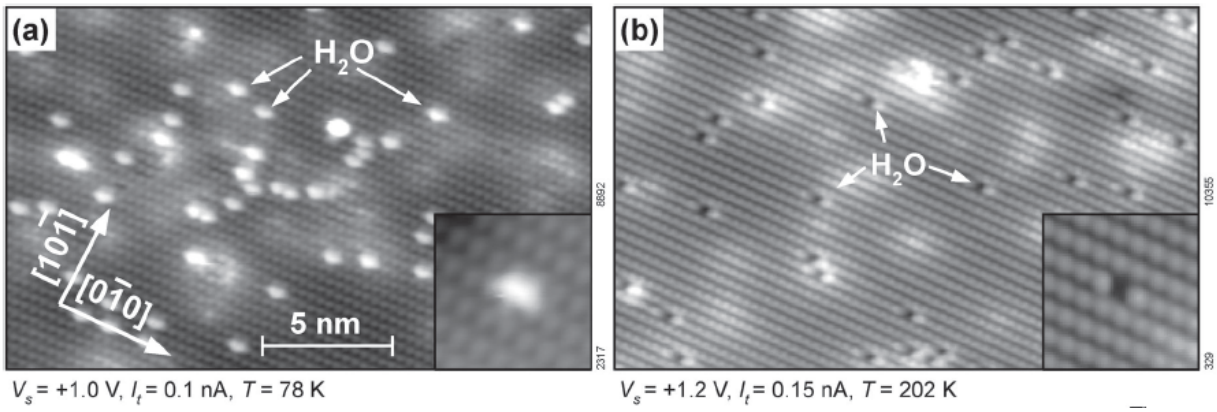

Fig.1. (a,b): 20 ×12 nm^2 STM images of anatase (101) after exposure to 0.01 L H_2O, dosed at T_{sample}= 120 K, scanned at (a) T_{sample}= 78K, (b) T_{sample}=202 K. Adapted from [95].

3.1.2 Dissociative and molecular adsorption of water on TiO_2 nanoparticles: insights from FT mid-IR (MIR) spectroscopy in controlled atmosphere

In the case of TiO_2 nanoparticles, terminations of the (101) type accounts for most part of their surfaces, but higher energy surfaces, like those of the (110) type are exposed, as well us edges and corners, where H_2O molecules are dissociated, forming hydroxy groups, which play an important role as scavenger of photogenerated holes, forming •OH radicals. As well known, the O-H stretching mode of such species produces a pattern in the 3800-3200 cm^{-1} range, highly informative on their local structure. The investigation of these features has been the subject of many papers [96-106] that have based the assignment of variousν(OH) bands on the pioneering work of Primet et al. [96] and Tsyganenko et al. [97]. Using these reports, ν(OH) bands at frequencies higher than 3680 cm^{-1}were assigned to linear hydroxy groups, while bands at lower frequencies were related to bridged -OH, the

two species resulting from the dissociation of H_2O on pairs of coordinatively unsaturated Ti^{4+} and O^{2-} surface sites. A more comprehensive assignment was proposed by Busca et al. for TiO_2 P25 (now by Evonik, formerly by Degussa) [99], and experimental data and theoretical calculations from Dzwigaj et al. explored the dependence of the ν(OH) pattern on the morphology of two types of anatase TiO_2 particles, focusing on regular faces [107]. Furthermore, in those experiments water molecules were present on the surfaces, and most of the observed ν(OH) bands were attributed to adsorbed H_2O. Notably, the investigation of structure−reactivity relationships of steps on anatase TiO_2 single crystals has been the subject of a combined experimental and theoretical study [108]. Data reported in [96] can be considered as an example of the possible overall appearance and evolution upon outgassing at increasing temperatures of mid-IR signals due to hydroxy groups and water molecules at the surface of titania nanoparticles, in this case P25. Fig. 2 shows the spectra of TiO_2 outgassed up to 773 K in the ν(OH) (section A) and δ(H_2O) (section B) ranges, which exhibited a general trend quite similar to that reported by Mino et al in his a work on pure nanoanatase [109].

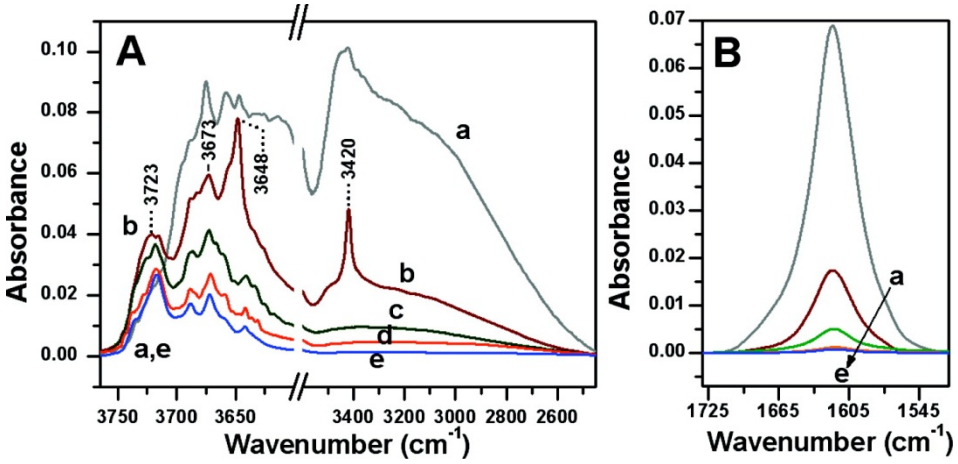

Fig. 2. IR spectra in the ν(OH) and δ(H_2O) regions (sections A and B, respectively) of TiO_2 P25 outgassed for 60 min at: (a) beam temperature, i.e., ca. 323 K, (b) 473, (c) 573, (d) 673, and (e) 773 K. On the *X* axis, the scale has been changed at 3600 cm^{-1}, to zoom the region at higher frequency. The gap on the axis is just of 1 cm^{-1}. Reprinted with permission from ref [110].

After degassing at beam temperature (curve a), the region at high frequencies was dominated by a broad and complex absorption spread over a range from 3600 to 2500 cm^{-1}, due to −OH oscillators involved in H-bonds, and accompanied by a series of narrow and partly resolved peaks/subbands in the 3600−3750 cm^{-1} range, related to −OH groups experiencing weaker intermolecular interactions (Fig. 2a). In experimental studies, bands in the latter range have been mostly assigned to hydroxy groups, whereas undissociated water molecules, coordinatively adsorbed on surface Ti^{4+} ions, mainly contributed to the 3600−2500 cm^{-1} absorption [101], other than produce the δ(H_2O) band at ca. 1620

cm^{-1} (Fig. 2b). However, more recent theoretical investigations proposed that H_2O adsorbed at high coverage, apparently not involved in H-bonds, should absorb in the 3750−3600 cm^{-1} range [111]. Nevertheless, the number of components in this range (at least 9, considering maxima and shoulders) indicated the presence of several types of surface sites bearing hydroxyl groups and adsorbed H_2O molecules.

The decrease in integrated intensity of the δ(H_2O) band after outgassing at 473 K (Fig. 2b) monitored the removal of approximately 75% of the adsorbed H_2O molecules. Water desorption and condensation of hydroxy groups were also responsible for the decrease in intensity of the ν(OH) pattern that occurred to a much higher extent for the broad 3600−2500 cm^{-1} band than for the set of sharp 3750−3600 cm^{-1} peaks. This latter now exhibits a main peak at 3648 cm^{-1}, asymmetric toward the lower frequency side and with a shoulder at 3655 cm^{-1}. Additionally, another component at 3673 cm^{-1} with subbands at 3690 cm^{-1}, and a new band with a maximum at 3723 cm^{-1}, resulting from the overlap of several components, appeared. This complex signal was assigned to O−H oscillators initially involved in H-bonding (and then absorbing at lower frequencies) with hydroxyl groups/water molecules that were removed by outgassing. Noticeably, a quite narrow band was now observed at 3420 cm^{-1}, still superimposed on a broad absorption. This band was supposed to be characteristic of the rutile phase present in the P25 [103], but was also observed for a pure anatase sample [101]. In this last case, it was assigned to coordinated water species on the basis of the similar evolution in dependence on the outgassing temperature with respect to the δ(H_2O) band. Conversely, in a more recent paper, this component was supposed to be due to hydroxy groups playing a special role in the photocatalytic behavior of the P25, but this assignment is questionable, because the δ(H_2O) spectral range was not reported [106]. In the present case, outgassing at 573 K (Fig. 2a,b, curves c) resulted in the depletion of the 3420 cm^{-1} band and in a decrease in intensity of the broad feature below, while the δ(H_2O) band appeared significantly weaker. This behavior might support the assignment of the 3420 cm^{-1} signal to water molecules. However, it must be considered that two ν(OH) absorptions were expected for H_2O molecules and that a partner signal must be identified. In addition, the location of the considered band was in the range typical for OH oscillators involved in H-bonds, and such interactions usually produce a significant broadening of the absorption profile (increasing as the frequency of the maximum is decreased). Furthermore, none of the frequencies calculated by Arrouvel et al. [111] for adsorbed H_2O fit with the band at 3240 cm^{-1}. As for the set of signals at higher frequencies, the main effect of outgassing at 573 K was the depletion of the 3648 cm^{-1} peak, accompanied by an overall decrease in intensity of the other components. Subsequent outgassing at increasing temperatures up to 773 K left only traces of the broad absorption in the 3600−2600 cm^{-1} region and resulted in a progressive decrease in intensity of the 3750−3600 cm^{-1} pattern (Fig. 2a).

As indicated above, the dissociation of H_2O molecules on TiO_2 anatase requires terminations with a surface energy higher than the (101) types. Since advances in titania nanoparticles with controlled shape and size TiO_2, the surface hydration, hydroxylation, Lewis acidity and photocatalytic Activity of TiO_2 anatase nanoparticles with dominant (001) type facets was investigated, also in comparison with "usual" TiO_2 anatase nanoparticles with a truncated bipyramidal shape, i.e. with dominant (101) type surface terminations [113]. The collection of data provided by several complementary techniques clearly indicated that after thermal removal of capping agents, i.e. F^-, to obtain a bare TiO_2 material, high energy (001) types terminations are not actually exposed at the surface of platy

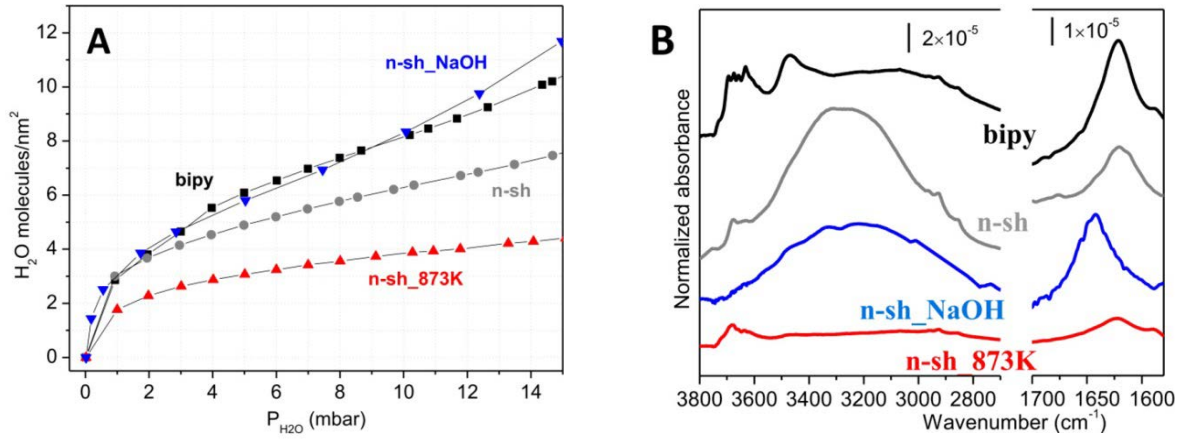

Fig. 3. (A) Water adsorption isotherms at 298 K obtained from microgravimetric measurements. The samples have been previously outgassed at room temperature. (B) IR spectra of the samples outgassed at r.t. for 1 h. In both panels labelling is as follows: n_sh (nano-sheets), pristine platy TiO2 mainly exposing (001) type facets; n-sh_NaOH, n_sh treated with a 0.01 M NaOH solution; n_sk_873K, n_sh calcined at 873 K; bipy (bipyramidal): TiO_2 nanoparticles mainly limited by (101) type facets. Adapted from ref. [113].

3.1.3 Superhydrophilicity of TiO_2 nanoparticles induced by UV light irradiation: insights from diffuse reflectance near-IR (NIR) spectroscopy

IR spectroscopy can be a useful tool for investigating the structure of multilayers of water molecules adsorbed on the surface of oxide nanoparticles, in particular when exploited in the near-IR, in order to analyse the features of the signal due to $\nu_{asym}+\delta$ combination mode of H_2O, highly sensitive to the interactions water molecule are involved in [114]. It is worth to notice that also the signals in the MIR range due to the fundamental stretching modes of H_2O show such sensitivity, but they suffer of the interference by those due to surface hydroxy groups. In particular, the overall decrease in intensity of the $\nu_{asym}+\delta$ signal due to water adsorbed at the surface of TiO_2 P25 nanoparticles in contact with air and exposed to UV light revealed that H_2O molecules adsorbed on the TiO_2 surfaces desorb during UV light irradiation by the heating effect of the light source (Fig. 4) [115]. Since the amount of the

H_2O adsorbed on the TiO_2 surfaces decreased, the distribution of the hydrogen bonds within the H_2O molecules decreased, resulting in a decrease in the surface tension of the H_2O clusters. This insight was obtained by fitting the experimental profile with sub-bands, which were assigned to H_2O molecules experiencing different intermolecular interactions. By adopting the labeling of sub-bands in Fig. 4 S0, H_2O molecules without any active hydrogen bonds; S1 and S2, H_2O molecules with one or two active hydrogen bonds; S*n*, polymeric chained H_2O clusters.

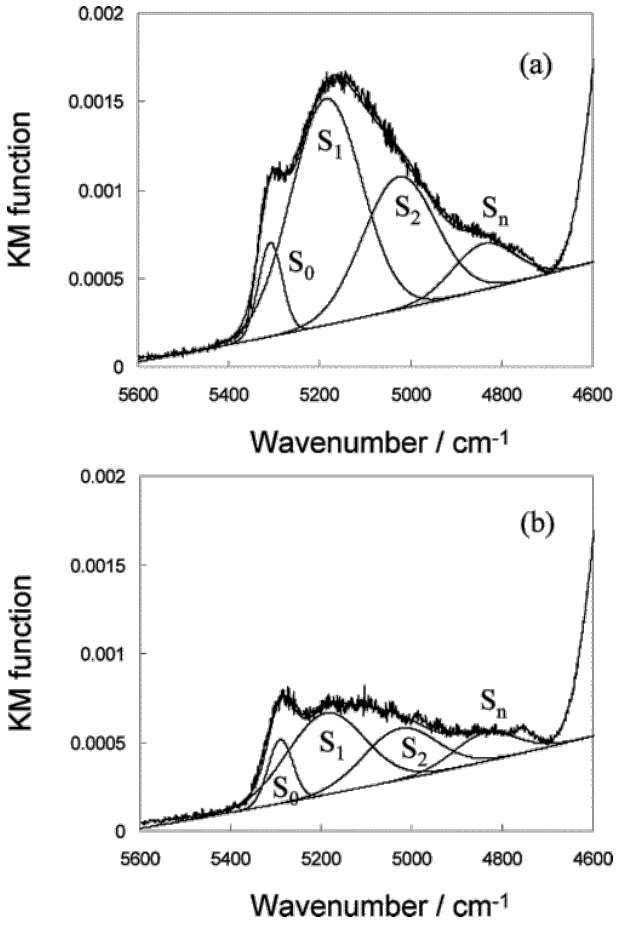

Fig. 4. Fitted combination (ν_{asym} + δ) sub-bands of H_2O molecules adsorbed on TiO_2 P25 nanoparticles exposed to air: (a) before UV light irradiation and (b) after UV light irradiation for 3 h. Reprinted with permission from ref. [115].

The decrease in the surface tension of H_2O under UV light irradiation was found to be one of the most important driving forces in which the H_2O clusters on the TiO_2 surface spread out thermodynamically, forming H_2O thin layers.

3.2 Carbon dioxide at TiO_2 surfaces

The CO_2 adsorption on TiO_2 is the first step in all the photoreduction processes described in the introductory section and different structures for the adsorbate can be identified [116]. As depicted in

Fig. 5, they can grouped in: i) linear structures (L); ii) monodentate carbonates (MC); iii) bidentate carbonates (BC), which can be bridging, if the carbonate is bound to two adjacent Ti centres, or chelating, if the bidentate bond is formed with a single Ti site; iv) monodentate and bidentate bicarbonates (MB and BB) obtained from the corresponding carbonate structures after interaction with water, which is a crucial co-reactant in many CO_2 photoreduction processes (for further details concerning the interaction of H_2O with TiO_2 *vide supra*).

Different characterization techniques (e.g. scanning probe microscopies, in situ spectroscopies, microcalorimetry, microgravimetry, temperature-programmed desorption) can be employed to investigate the surface processes occurring during CO_2 adsorption and subsequent reactions. In our contribution we will mainly focus on vibrational spectroscopy combined with ab initio calculations.

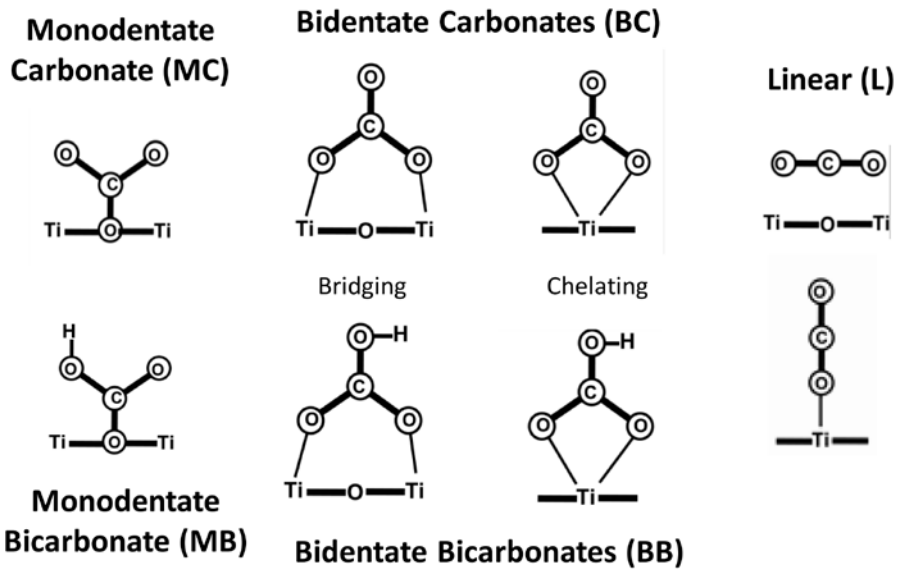

Fig. 5. Possible surface structures resulting from the interaction of CO_2 on TiO_2. Unpublished Figure.

3.2.1 Single crystal investigations of CO_2 adsorption on TiO_2

Concerning single crystal investigations of CO_2 adsorption, the rutile (110) surface, being the most stable and easy to obtain, has been the most studied. By combining ultra-high vacuum (UHV) FTIR spectroscopy and DFT calculations Cao et al. [117] showed that at 90 K on the reduced (110) surface CO_2 is first adsorbed on oxygen vacancy (V_O) sites, then on the five-coordinated Ti cations (Ti_{5c}) sites and finally on bridging oxygen (O_{br}) sites. Also several computational studies were devoted to the CO_2-rutile (110) system employing different levels of theory from semiempirical Extended

Huckel Molecular Orbital calculations on small rutile clusters [118] to very accurate wave-function-based ab initio methods [119]. For instance, Kubas et al. [119] obtained quantitative agreement with respect to the experiment for CO_2 adsorption geometry and binding energy (within 1 kcal/mol) using "gold standard" coupled-cluster calculations with single, double, and perturbative triple excitations, CCSD(T), extrapolated at the complete basis set limit.

Single crystal data on anatase TiO_2 are less abundant and are mainly focused on the most stable (101) surface. Cao et al. [120] combined UHV FTIR spectroscopy and ab initio molecular dynamics to demonstrate that at 90 K adsorbed CO_2 does not keep a stationary adsorption state but shows a swing motion. In particular, one side of the linear CO_2 molecule is bound to a surface Ti_{5c} site, while the other end swings within the (010) plane being tilted with respect to the [10-1] direction of an angle ranging from 10° to 60°.

3.2.2 Study of CO_2 adsorption and reactivity on TiO_2 nanoparticles

Experimental results obtained on powdered anatase TiO_2 samples are more copious and report the formation of several different carbonate or bicarbonate species (if co-adsorbed water is present) after CO_2 adsorption (see Fig. 5). However, a precise assignment of the different components present in the vibrational spectra is not straightforward, especially for commercial anatase/rutile mixtures, like the famous Evonik (Degussa) TiO_2 P25 [121, 122]. Mino et al. [116] combined FTIR spectroscopy and periodic DFT calculation to better elucidate the role of the different surface sites in the CO_2 adsorption and reactivity on both dehydrated and hydrated TiO_2 anatase nanoparticles. They showed that CO_2 is weakly adsorbed in molecular form at the most stable (101) surface. Conversely, the formation of carbonate and bicarbonate species is favoured at the (001) surface owing to the stronger (Lewis and Brønsted) basicity of its surface oxygens. Similar processes occur on the low coordinated sites present on high index facets and on steps, edges and corners [123]. The authors also created simulated IR spectra using the vibrational frequencies obtained from the DFT calculations for the most stable CO_2 surface structures. As visible in Fig. 6a, for dehydrated surfaces a good agreement with experimental spectra is obtained considering the presence of linear CO_2 molecules on the (101) surface and monodentate carbonate species on the (001) surface. Conversely, when CO_2 is adsorbed on partially hydrated TiO_2 nanoparticles, different monodentate and bidentate bicarbonates are formed on (001) facets and on low coordinated sites (Fig. 6b). These findings show that a controlled variation of the exposed anatase surfaces, exploiting shape-engineered nanoparticles [124], can modify the reaction paths and improve the final CO_2 reduction performance [125].

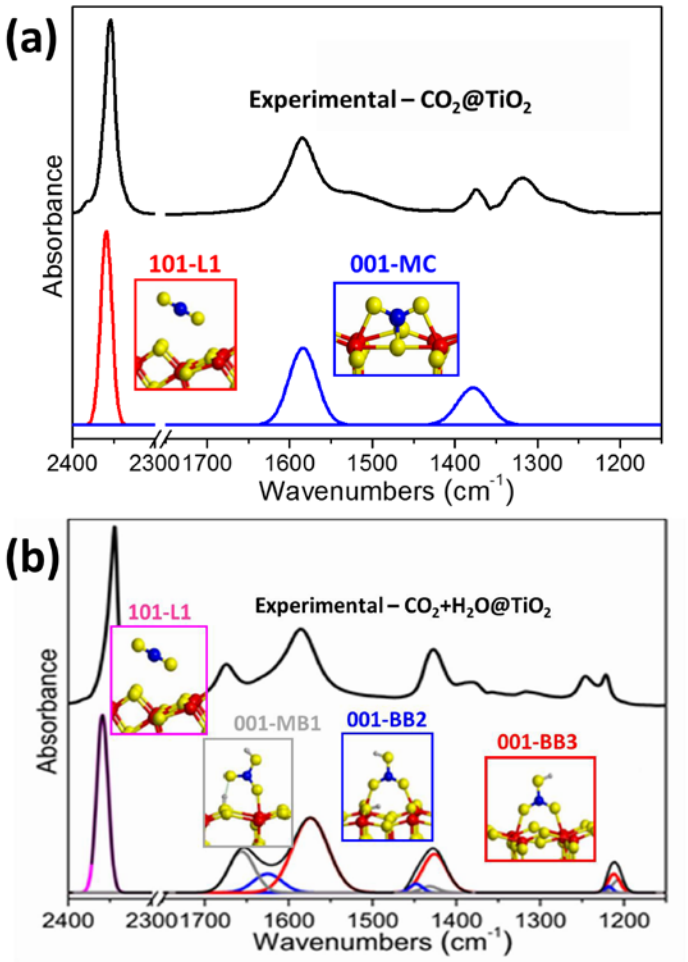

Fig. 6. (a) Comparison between experimental and simulated IR spectra constructed employing computed IR data for dehydrated anatase surfaces, highlighting the presence of linear CO_2 molecules on the (101) surface (101-L1) and monodentate carbonate species on the (001) surface (001-MC). (b) As part (a), for partially hydrated anatase surfaces: in presence of co-adsorbed water, monodentate bicarbonates (001-MB1) and two different kinds of bidentate bicarbonates (001-BB2 and 001-BB3) are formed on the (001) surface. Unpublished Figure reporting results published in ref. [116].

Some researchers employed vibrational spectroscopy to investigate also the effect of UV-Vis irradiation on the CO_2 reactivity at the surface of TiO_2 nanoparticles [126-129]. Liu et al. [126] studied the photocatalytic CO_2 reduction in presence of water on different TiO_2 polymorphs by diffuse reflectance infrared Fourier transform spectroscopy (DRIFTS). They monitored in dark conditions the evolution of the surface species after dosing CO_2 and H_2O on anatase nanoparticles noticing the initial formation (after 0-5 minutes) of CO_2^-, HCO_3^- and bidentate carbonates, followed by their decrease with a parallel growth of the water bending signal after 15 minutes (Fig. 7a). UV-Vis irradiation (see Fig. 7b) induced the reappearance of the CO_2^- signals (1675 and 1249 cm^{-1}) and

a progressive increase of the bicarbonate (1415 and 1221 cm^{-1}) and bidentate carbonate (1583 and 1345 cm^{-1}) bands. This behavior suggests that the surface allows the photoexcited electrons, previously trapped in defect sites, to be transferred to the adsorbed CO_2. They also proposed a possible reaction pathway for the formation of carbon monoxide and methane from CO_2 photoreduction in presence of water vapor on oxygen-deficient anatase and brookite TiO_2 phases, which is reported in Fig. 7c.

Finally, Wang et al. [128] investigated dispersed CeO_2/TiO_2 and bare TiO_2 anatase samples showing that, unlike monodentate carbonates, bidentate carbonates and bidentate bicarbonates could be readily transformed to surface CO_2^- in the presence of H_2O under simulated sunlight irradiation.

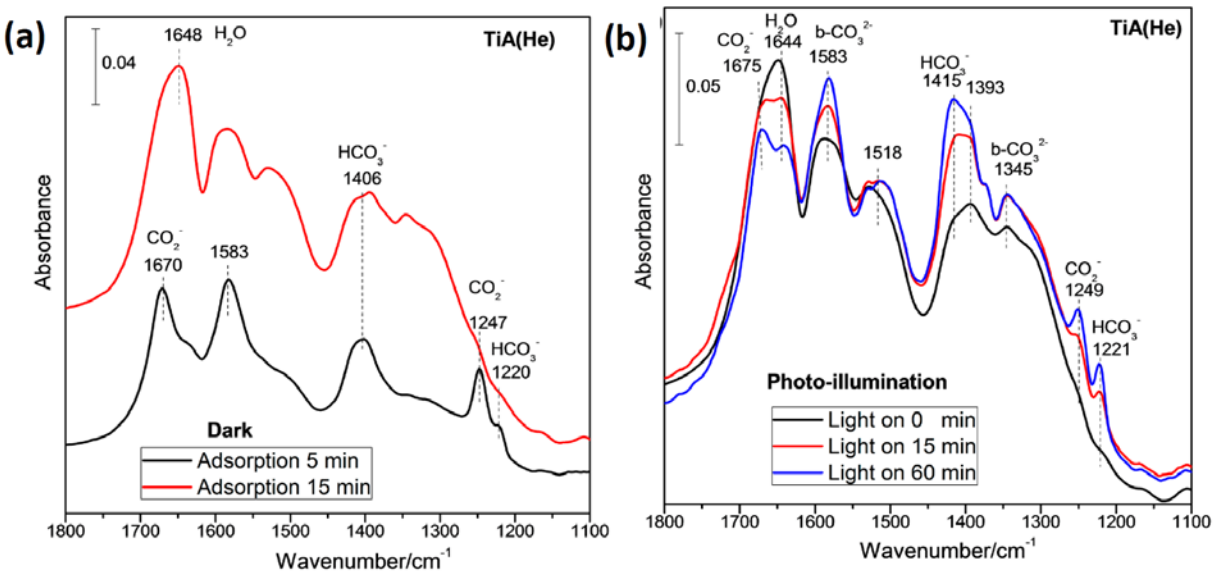

(c)

$$H_2O + h^+ \rightarrow H^+ + OH\bullet \quad (1)$$

$$CO_2 + Ti^{3+} \rightarrow Ti^{4+}\text{–}CO_2^- \quad (2)$$

$$OH\bullet + CO_2^- \rightarrow HCO_3^- \quad (3)$$

$$CO_2^- + H^+ + e^- \rightarrow CO + OH^- \quad (4)$$

$$CO_2^- + CO_2^- \rightarrow CO + CO_3^{2-} \quad (5)$$

$$CO_2^- + [Ti^{3+}\text{–}V_O\text{–}Ti^{4+}] \rightarrow CO + [Ti^{4+}\text{–}O^{2-}\text{–}Ti^{4+}] \quad (6)$$

$$CO, HCO_3^-, HCOOH \xrightarrow{e^-} C_{(ads)}\cdot \xrightarrow{H\bullet} CH_3\cdot \xrightarrow{H\bullet} CH_4 \quad (7)$$

Fig. 7. In situ DRIFT spectra of CO_2 interaction, in presence of H_2O, with anatase TiO_2 (a) in the dark and (b) after subsequent UV-Vis irradiation as a function of time. (c) Possible reaction pathway for the formation of CO and CH_4 from CO_2 photoreduction on defective (non-stoichiometric) anatase and brookite TiO_2 phases. Reproduced with permission from ref. [126].

3.3 Heterostructures at TiO_2 surface as organic sensitizers

3.3.1 The acetylene/ TiO_2 interaction

The surface chemical properties of an oxide are primarily related to the nature of the exposed coordinatively unsaturated sites in terms of the Lewis basicity of the O^{2-} anions and of the Lewis acidity of the M^{n+} metal sites (as well as of the Brønsted acidity of residual OH groups, if present) [130-132]. From this point of view, the $Ti^{4+}O^{2-}$ pairs present at the TiO_2 surface are usually considered to have weaker Lewis acidity and basicity with respect to oxides like MgO or Al_2O_3, which are for instance highly effective in the dissociative adsorption of a weak acid molecules like acetylene to give $M^{n+}(^{-}C{\equiv}CH)$ and OH^- species [133]. It is however a matter of facts that due to its semiconductor nature TiO_2 can take advantage of other characteristics which are absent on insulators like MgO or Al_2O_3: one is obviously the reduced band gap (at the basis of the photoactivity) while the other is represented by the redox properties of the Ti^{n+} centres. As we will see in the following, the reactivity of acetylene (and in general of alkynes) at the TiO_2 surface depends mostly on the redox properties of the metal centres rather than on the Lewis properties. Other important factors are the nature of the TiO_2 polymorph used as substrate (rutile or anatase) and the nature of the exposed crystallographic faces.

Starting with the studies devoted to the interaction with the well-defined surfaces of single crystals, the adsorption from the gas phase of alkynes of general formula $RC{\equiv}CH$ (R = H or CH_3) at the (001) surface of rutile has been systematically studied by Barteau *et al.* [134, 135]. Stoichiometric (completely oxidized) samples result to be completely inactive. On the contrary, the same surface partially reduced by sputtering and hence containing a discrete concentration of Ti^{2+} sites, shows a marked tendency to trimerize acetylene to benzene as main product (with smaller amounts of dienes and olefins formed respectively by dimerization and hydrogenation side reactions).

3.3.2 Role of the TiO_2 surface sites in affecting the oligomerization/condensation mechanisms

The reaction mechanism proposed for acetylene is shown in Scheme I: after the initial adsorption of two C_2H_2 molecules on the reduced Ti^{2+} sites a cyclic intermediate is formed where Ti^{2+} is temporarily oxidized to Ti^{4+}. Subsequent insertion of a further acetylene molecule leads to trimerization with formation of adsorbed benzene (desorbed at about 400 K) and the closure of the catalytic cycle by reduction of the metallic centre from Ti^{2+} to Ti^{4+}.

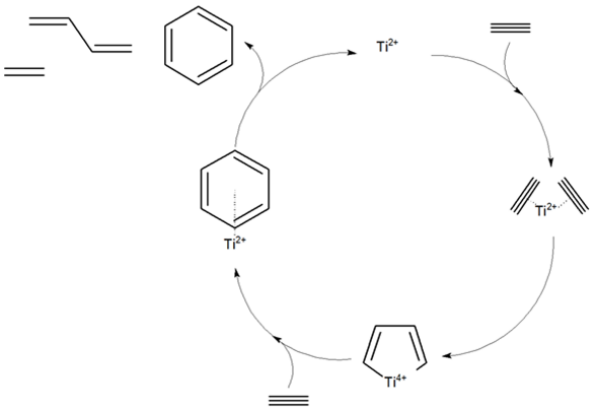

Scheme I. Mechanism of the acetylene trimerization reaction on the face (100) of TiO_2 rutile single crystal. Adapted from ref. [134].

Trimerization to benzene is also the main reaction observed on dehydroxylated (by outgassing in vacuo at 773 K) nanocrystalline TiO_2 P25 Degussa (now Evonik), a material consisting as well-known of an anatase and rutile mixture in *ca*. 3: 1 proportion [136].

The formation of benzene is on the contrary not reported by Rives-Arnau and Sheppard [137] who have studied by Raman spectroscopy the HC≡CH interaction with polycrystalline rutile samples (mean size *ca*. 10 nm) obtained by hydrolysis of $TiCl_4$. The main reaction observed at room temperature on these nanocrystals, which are supposed to preferentially expose (110) terminations, is actually the acetylene oligomerization to form linear *trans*-polyacetylene chains.

By comparing the absorption frequencies of the $\pi \rightarrow \pi^*$ optical transition with the vibrational frequencies of the $\nu_{C=C}$ stretching mode of the obtained products and with the position of the absorption maxima in the electronic spectra of a series of polyenes containing a known number of conjugated double bonds, the authors conclude that the Raman bands they observe in the 1650-1500 cm^{-1} region witness the formation of a mixture of oligomeric chains containing up to a maximum of 20 conjugated double bonds. Chains of this length have absorption in the red region of the spectrum which explains the blue colour of the samples. Despite the use of different solvents, it was not possible for the authors to extract the products and hence to separate them from TiO_2, as can expected for chains anchored to the TiO_2 surface by chemical bonds. Based on these results, this study can be regarded as an early example of the preparation of a hybrid material consisting of a photoactive oxide covered with antenna molecules capable of absorbing radiation in the Vis region.

As far the reaction mechanism is concerned, the four and five coordinated Ti^{4+} sites present in equal numbers on the predominant faces (110) of the rutile nanocrystal are thought to be only the precursor

of the true active sites [138]. Because of the adopted activation procedure prior dosage of acetylene (*i.e.* outgassing at 723 K to dehydroxylate the surface and subsequent cooling in vacuum) it is in fact expected that TiO_2 loses oxygen with the consequent reduction of a considerable fraction of the Ti^{4+} centres to highly unsaturated Ti^{3+}, responsible for the acetylene oligomerization. As represented in Scheme II the oligomeric chains are supposed to start on certain site and to end on a neighbour, thus explaining the limited length (up to 20 conjugated double bonds) of the final *trans*-polyacetylene chains.

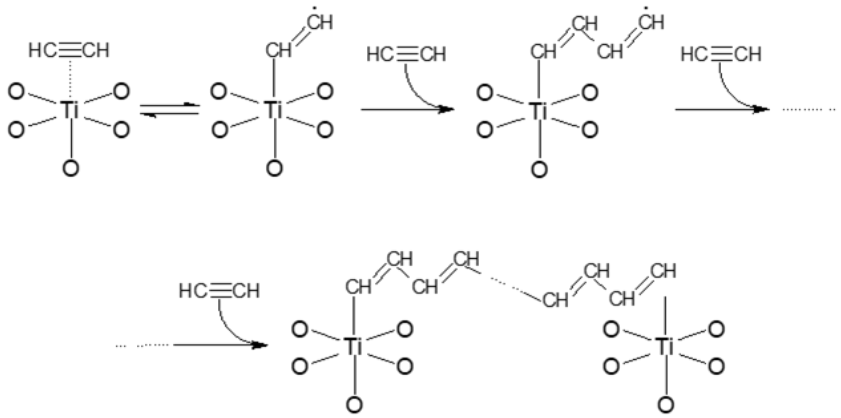

Scheme II. Acetylene oligomerization mechanism of on nanocrystalline TiO_2 rutile. Adapted from ref. [138].

3.3.3 The case study of acetylene TiO_2 P25 interaction via FTIR and EPR spectroscopies

Some of us have recently reconsidered the interaction of with TiO_2 P25 samples by a detailed investigation (by means of vibrational IR and Raman and UV-Vis diffuse reflectance spectroscopies) of the effects of the gas pressure, the contact time and the temperature on the C_2H_2/TiO_2 interaction [139]. It resulted that these parameters play a very important role in the distribution of the reaction products. In particular, IR spectroscopy highlighted that trimerization to benzene is main reaction channel for acetylene equilibrium pressures up to 10 mbar, as demonstrated by the appearance of the typical manifestations of aromatic CH stretching modes in the 3100-300 cm^{-1} region and of ring deformations modes at *ca.*1480 cm^{-1} (Fig 8). The very intense band at 3225 cm^{-1} and the weak one at 1950 cm^{-1} are also noteworthy as they are due respectively to the ≡C-H and C≡C (inactive in the free molecule) stretching modes of acetylene largely adsorbed on the nanocrystal surfaces. Both adsorbed acetylene and benzene are immediately desorbed by degassing at 293 K.

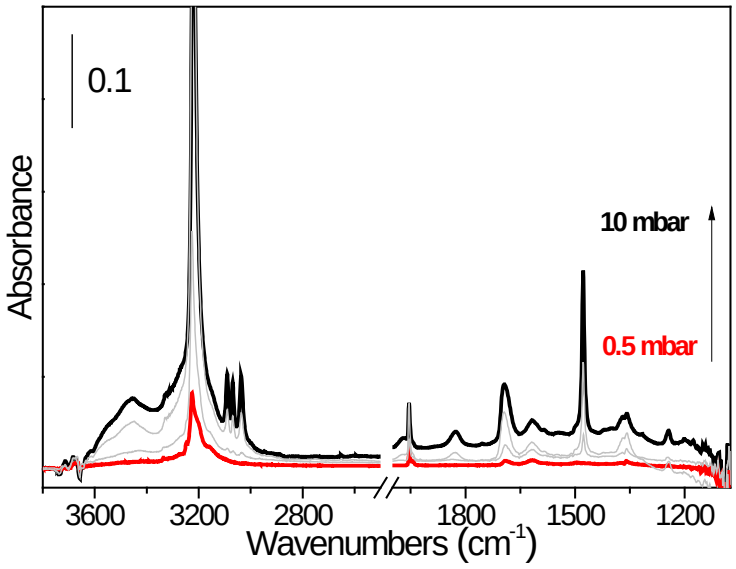

Fig. 8: Background subtracted IR spectra of acetylene adsorbed at low pressure (up to 10 mbar) on activated (outgassed at 773 K) and fully oxidized TiO_2 P25. Adapted from ref. [139]

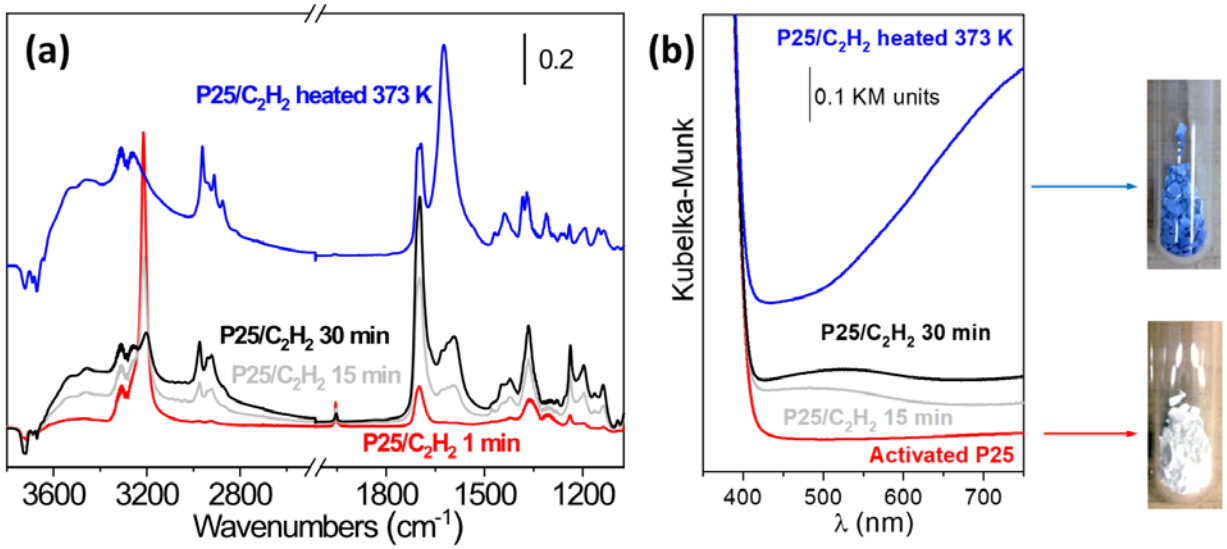

Fig. 9. (a) Background subtracted IR spectra of C_2H_2 adsorbed at 100 mbar on activated TiO_2 P25. The bottom series shows the evolution with the contact time at 293 K (red curve: immediately after acetylene dosage from the gas phase. Grey and black curves: after 15 and 30 min.) The blue spectrum is the result of increasing the temperature up to 373 K in C_2H_2 atmosphere. (b) UV-Vis spectra of the pure activated TiO_2 sample; the other spectra were obtained in the same contact time and temperature conditions of part a. The pictures in the right part are those of the activated solid and of the same sample after the thermal treatment at 373 K in acetylene. The dramatic change in color due to formation of conjugated and condensed reaction products is evident. Adapted from ref. [139]

The manifestations of adsorbed acetylene are still present when acetylene is dosed at higher pressures (> 100 mbar), but those due to benzene become extremely weak (Fig. 9a), suggesting that its formation is depleted in the actual experimental conditions. Instead, new spectral features develop with contact time (and by heating at 373 K in acetylene atmosphere) consisting of: (i) medium intensity bands in the 3000-2800 cm^{-1} region which indicate the formation of relevant amounts of saturated CH groups (mainly $–CH_3$ and to a lesser extent $–CH_2$); (ii) a broad absorptions in the region 3650-3250 cm^{-1} suggesting the formation of OH groups perturbed by hydrogen bonding and (iii) the progressive growth of complex features in the region below 1750 cm^{-1} due to the formation of highly unsaturated products containing an extensive system of conjugated double bonds. Notably, the formation of these products is paralleled by the progressive decrease of the intensity of the bands due to physically adsorbed acetylene, which is consumed in the process. The hypothesis of progressive growth of products containing an increasing number of conjugated double bonds is confirmed by the optical spectra in Fig. 9b, where the development of a broad absorption gradually shifting from the UV-Vis towards the NIR is observed, which is consistent with the dramatic change in colour of the sample from white to intense blue. The colour does not disappear by exposure to the atmosphere, thus excluding that it is only due to formation of reduced Ti^{3+} species, or to the treatment of the sample with organic solvents, thus suggesting that the responsible products are strongly adsorbed on the TiO_2 surface. The contemporary formation of –O-H and saturated, hydrogen rich, $–CH_3$ (and $–CH_2$) moieties and conjugated double bonds cannot be accounted for by supposing the formation of linear polyacetylene chains as in ref. [138], which would maintain the 1:1 C:H ratio of the free C_2H_2 molecule. Instead, it is fully justified by a concerted mechanism in which the extraction of hydrogen to form OH and methyl or alkyl groups is accompanied by self-assembling of the carbon-rich acetylene residues to form condensed products of high molecular weight, as shown in Scheme III.

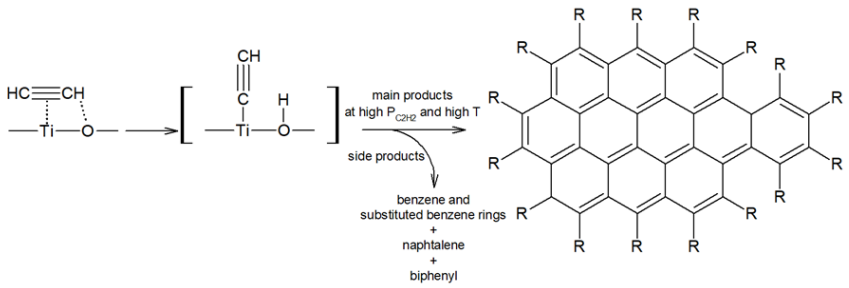

Scheme III. Schematic representation of the reaction pathway of acetylene on TiO_2 P25. R = H, CH_3, alkyl groups. Adapted from ref. [139].

In a subsequent work the interaction of C_2H_2 with P25, anatase and rutile TiO_2 was studied for the first time by EPR spectroscopy [140]. In all cases upon acetylene dosage on highly dehydroxylated samples the appearance of EPR signals undoubtedly associated with the formation of reduced Ti^{3+} species is observed. This significant result allows to better detail the mechanism leading from acetylene coordination (first step in Scheme III) to the formation of the final condensed products. While excluding homolytic dissociation of the HCC-H bond (unlikely in the actual reaction conditions), it is hypothesized that the reduced Ti^{3+} centres are formed by electron transfer from a HCC^- acetylide fragment formed, by ≡C-H heterolytic dissociation (with parallel formation of OH groups as evidenced by the IR spectra: *vide supra*), to the solid whose propensity to reduction is well documented. The initial phases of the reaction can therefore be summarized as:

$$HC{\equiv}CH_{(g)} + Ti^{4+}\text{-}O^{2-} \rightarrow HC{\equiv}CH_{(ads)} + Ti^{4+}\text{-}O^{2-} \rightarrow [HC{\equiv}C^-_{(ads)}Ti^{4+}\text{-}OH^-] \rightarrow HC{\equiv}C^{\bullet}_{(ads)}Ti^{3+}\text{-}OH^-$$

where Ti^{4+}-O^{2-} represents Lewis acid/base pairs at the TiO_2 surface. The HCC· species would then be responsible for the formation of simple condensed products, such as naphthalene, as it follows:

$$3C_2H_2 + 2HC{\equiv}C\cdot \rightarrow C_8H_{10}$$

The ability of the surface to accept protons, because of the basicity of the surface O^{2-}, and at a much larger extent the propensity of the solid to accept electrons can then be imagined as the driving forces for the formation of highly unsaturated, condensed products (with C:H >>1 ratios) and of saturated groups, according to mechanisms like those in Scheme IV:

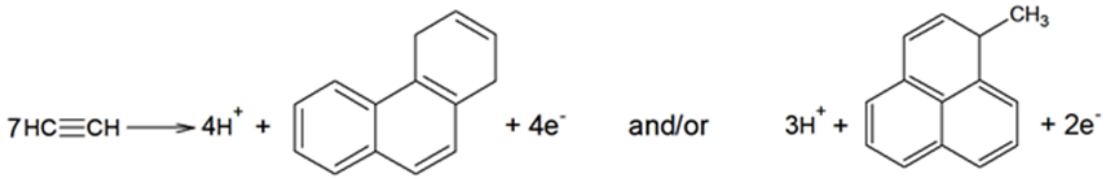

Scheme IV. Schematic representation of the possible pathways leading to formation of condensed aromatics products by interaction of acetylene with TiO_2. The side products protons and electrons are captured at the solid surfaces to form surface hydroxyls and reduced Ti^{3+} centres. Adapted from ref. [140].

The validity of the reaction pathways proposed in refs. [139] and [140] and summarized in the above schemes has been recently supported by DFT (Density Functional Theory) simulations of the interaction of acetylene with the (101) and the less stable (001) surfaces of anatase [141]. Both the faces result to be fully inactive when saturated with OH groups, while after dehydroxylation they gain

the ability to adsorb the acetylene molecules through dispersive forces (physical adsorption). Nevertheless, the more stable (101) face is still chemically inactive, being unable to promote the acetylene dissociation. It also results inactive toward the simple acetylene trimerization reaction to benzene, even when reduced Ti^{3+} centres are introduced by simulating oxygen vacancies.

The calculations reveal a radically different behaviour of the less abundant and less stable (001) faces. It is for instance found that on this surface the an entire sequence of reactions, finally leading to formation of naphthalene, supposed to go through: (i) C_2H_2 adsorption, (ii) heterolytic dissociation on TiO pairs, (iii) insertion of a first C_2H_2 molecule in the C_2H^- fragment to form a four-membered $C_4H_2^{2-}$ chains, (iv) insertion of a further molecule to form a C_6H_4 ring anchored to the surface by σ bonds between the two terminal C atoms and two Ti centres and (v) insertion of two more acetylene molecules to form strongly adsorbed naphthalene (C_8H_{10}), is energetically favoured.

The overall reaction can be summarized as:

$$5C_2H_{2(g)} + 2Ti^{4+}{}_{(s)} + 2O^{2-}{}_{(s)} \rightarrow C_{10}H_{8(ads)} + 2Ti^{3+}{}_{(s)} + 2OH^{-}{}_{(s)}$$

where the need for the contemporary formation of condensed (conjugated) products, surface hydroxyls and reduced Ti^{3+} species well account for the IR, UV-Vis and EPR results in refs.[139] [140].

The hypothesis advanced by some of us in ref. [139] that reaction of acetylene with the TiO_2 surface in controlled experimental conditions could represent a useful route for the *in situ* preparation of graphene layers (possibly acting as stabilizers of the photo excited electrons) has recently found an experimental verification in the work of Shao, Zhang and co-workers [142, 143]. By using an acetylene gas flow in presence of H_2 excess and Ar as carrier, they were in fact successful in growing (at 923 K) highly uniform graphene layers (including single- and bi-layers) directly and at the surface of rutile TiO_2 single crystals [143] and anatase TiO_2 nanosheets [142].

This CVD strategy allows to maximize the photocatalytic activity of the graphene/TiO_2 hybrid with respect to other preparation procedures (see the references quoted in the introduction for their description) because avoids the formation of interfacial contaminates and ensures a better contact uniformity between the two phases. These unique characteristics allowed a more precise investigation of the dynamic of the charge transfer at the interface under illumination. In this respect, ultrafast transient absorption (TA) measurements performed under ambient conditions showed that the average lifetime of the photoexcited electrons depends on the time of the CVD reaction (and in turn on the extension of the surface graphene layer) following a volcano curve. The maximum of the curve is obtained by covering the surface of the TiO_2 nano-sheets by a continuous and uniform single layer.

In this condition the lifetime is nearly double with respect to pure TiO_2. A volcano curve is also observed as far the photocatalytic activity is concerned, but the maximum is now observed for a bilayer. The discussion of the reasons of these apparently conflicting differences is outside the scope of this review and the reader is referred to the original papers for details.

3.4 Heterostructures at TiO_2 surface as inorganic sensitizers

3.4.1 MoS_2/TiO_2 heterostructures: the role of the interface

In order to take on the challenges and the opportunities of new applications, the understanding of the relationship between structure and properties of many MoS_2/TiO_2-based heterostructures, obtained through different synthetic strategies, including *ex-situ* and *in-situ* approaches becomes essential. Concerning the *ex-situ* method, the MoS_2 and/or TiO_2 materials are fabricated in advance and then they are combined together by impregnation, drop-casting, ultrasonication, ball-milling, sol-gel or hydrothermal/solvothermal methods [62, 86]. The main advantages of the *ex-situ* methods are low cost and scalable production, but multiple steps are required and, more notably, highly heterogeneous MoS_2/TiO_2-based composites with weak interface interactions are often obtained. Conversely from the *in-situ* methods, which are based on chemical reactions occurring simultaneously or in different steps, composites with strong interface contacts can be achieved, with a more uniform dispersion, although at a low yield [62]. However the relatively small crystal mismatch (<5%) between TiO_2 (i.e. anatase and rutile) and MoS_2 structures [62] can help in the assembling peculiar TiO_2-based structures, thus achieving a satisfactory interface contact without aggregation. [144-147]. As for the lattice mismatch, that is, the different lattice constants and atomic arrangements between MoS_2- and TiO_2-based supports, [144-146] the above mentioned role of the interface, in affecting the charge transport phenomena or the catalytic processes, which in turn are depending on the nature and atomic structure of the active sites, has to be highlighted. Therefore by designing model systems of controlled morphology, the interface structure and then the charge control can be properly tailored. [148]. In the following we have chosen a few case studies in order to highlight the role of the interface structure in affecting the peculiar functionalities of the obtained architectures.

3.4.2 MoS_2/TiO_2 case studies via ex-situ and in- situ approaches

It is known that, due to the layered nature and flexibility of MoS_2 slabs, one or few-layer thick, the preferred orientation of the MoS_2 on TiO_2 surfaces is along the basal planes, thus minimizing the surface energy [149]. As such configuration leads to a low exposure of the active edge sites, which are more conductive than the basal planes, the possibility of making MoS_2 standing on the TiO_2, *e.g.* connecting the edges of few layer MoS_2 gives rise to a more effective heterostructure to improve photocatalytic hydrogen evolution, due to a better charge transport pathway [71]. Concerning this

point, He and co-authors reported a strategy to control the MoS_2 slab orientation on the TiO_2 facets by using *ex-situ* method (hydrothermal method) and two steps *ex situ/in situ* methods (CVD). Starting from MoO_2-decorated anatase fibres, the authors were able to manipulate the nucleation and growth processes of MoS_2 in such a way that according to the different approaches, MoS_2 particles, differently oriented with respect the TiO_2 support, were obtained. In particular, from the hydrothermal method MoS_2 arranged with the basal planes, whereas from CVD method MoS_2 arranged perpendicular to the basal planes on TiO_2 surface were, respectively, obtained. This is schematized in Fig. 10.

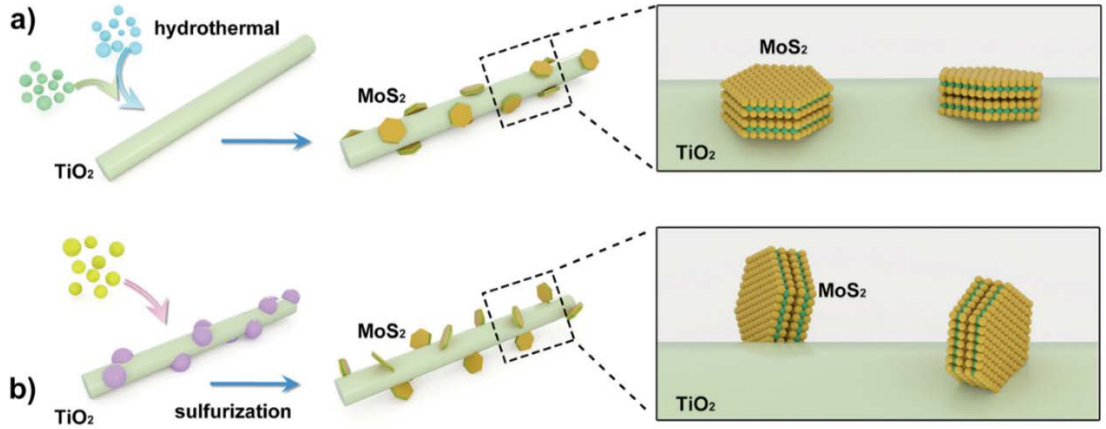

Fig. 10. Schematic representation of the MoS_2/TiO_2 preparation: a) by wet chemical method (MoS_2 arranged on TiO_2 surface with the basal planes), b) by CVD (MoS_2 arranged on TiO_2 surface perpendicular to the basal planes). Reproduced with permission from ref. [71]

More recently, Lin et al. [80] showed the fabrication of 2D nano-photocatalysts MoS_2/TiO_2 with a tuneable decoration amount of layered MoS_2 nanosheets via *ex-situ* two steps hydrothermal methods. The resulting MoS_2/TiO_2 heterostructures were HRTEM imaged (Fig. 11a) and mapped with elemental analysis (Fig. 11b). Notably, two kinds of lattice fringes, 0.62 nm and 0.35nm spaced, corresponding to the (002) planes of MoS_2 and to (101) planes of anatase TiO_2, were found (Fig. 11a). From the EDAX maps (Fig.11b), the elemental distribution of Ti, O, Mo and S was evidenced Taken together, these findings corroborate the decoration of TiO_2 nanoparticles by curved MoS_2 sheets, made by layered basal planes. Some more the optimal MoS_2 loading to give the best performance either for photocatalytic degradation or hydrogen production was determined to be 10 wt%, thus confirming the synergistic effect between MoS_2 and TiO_2, which accelerates the separation and migration efficiency of charge carriers, as well as enhances the light-harvest efficiency [80].

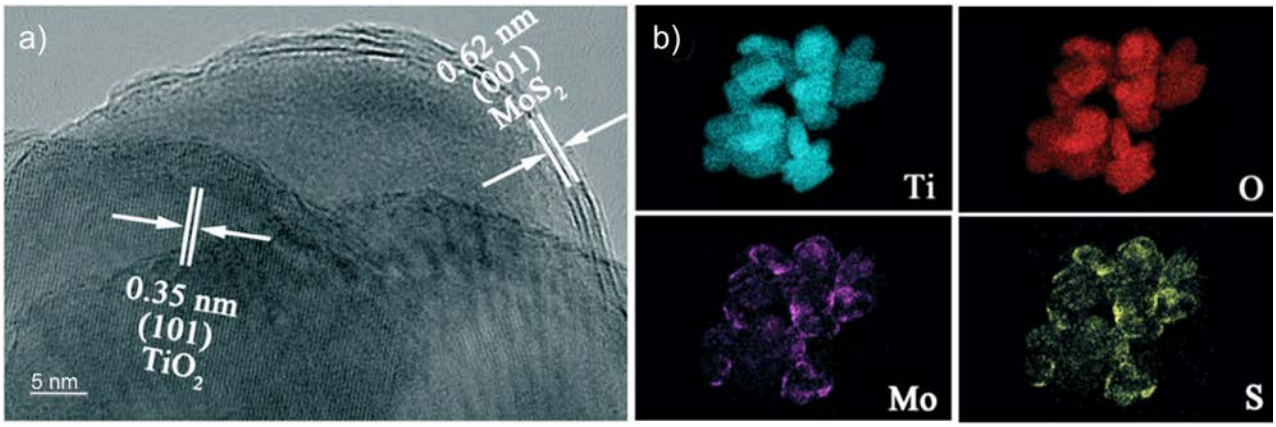

Fig. 11. a) HRTEM image of a MoS_2-decorated TiO_2 particle showing the MoS_2-TiO_2 interface; b) Ti, O, Mo and S elemental mapping of MoS_2-decorated TiO_2. Reproduced with permission from ref. [80].

However, irrespective of the stacking degree, the curvature of the MoS_2 slabs at the surface of some oxides (SiO_2, Al_2O_3, MgO, TiO_2 and titanate nanotubes) [144, 147, 150] has been observed rather frequently being depending primarily on the nature of the interaction of MoS_2 with the support, and on the type of defects (i.e. vacancies and dislocations) at the surface. As matter of fact, considering composites prepared also via *in-situ* and bottom-up approach, the authors observed that the MoS_2/support interactions increase from SiO_2 to γ-Al_2O_3 to TiO_2 until to MgO, which means that such interaction is maximized when MoS_2 slabs "act as chemical ligand" with a mutual phase reactivity [150]. A MoS_2/TiO_2 composite (36wt% Mo) recently obtained also via *in-situ* strategy with a bottom-up MoS_2 growth is illustrated in Fig. 12a. MoS_2 nanosheets were obtained by Scarano and co-authors [147] at the surface of anatase via the sulfidation of MoO_x-grafted titanate nanotubes. In this work, the authors took advantage of both, the thermal transformation of titanate nanotube into anatase nanoparticles and the contemporary sulfidation with CS_2. From the FTIR spectra of CO adsorbed at 100 K at decreasing coverage on the MoS_2/TiO_2 surface, (Fig. 12b), the following features can be briefly summarized: i) the band at 2180 cm^{-1} shifting at 2190 cm^{-1} at low coverage and the shoulder at 2166 cm^{-1}, which can be associated with (101) and (001) TiO_2 surfaces, respectively; ii) the disappearance of the band at 2113 cm^{-1}, associated with CO adsorbed on the reduced Mo^{x+} centres ($x < 4$). As discussed by the authors, the presence of reduced Mo^{x+} centres is related to sulfur vacancies on highly defective situations during the formation of the sulfide phase. Based on these results, the presence of MoS_2-decorated TiO_2 particles was also confirmed, and additionally AFM imaged (Fig. 12c). From this figure, a surface characterized by irregular hills and valleys can be highlighted.

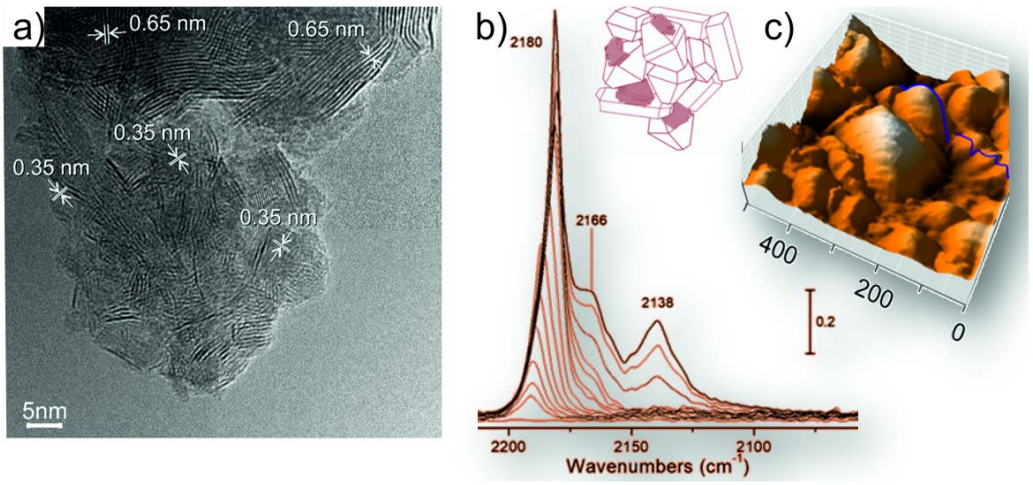

Fig. 12. MoS_2/TiO_2 sample obtained by the *in-situ* approach: (a) HRTEM image of few-layer MoS_2 sheets extensively covering the TiO_2 anatase particles. (002) planes of MoS_2 and (101) planes of anatase are reported; b) FTIR spectra of CO adsorbed at 100 K at decreasing coverage on the sample surface after sulfidation with CS_2 at 673 K, reduction with H_2 and re-sulfidation with CS_2; c) 3D AFM image of the same surface is characterized by irregular hills and valleys, where along a selected line the presence of few-layer thick MoS_2 slabs can be detected. Reproduced with permission from ref. [147].

In order to obtain more ordered systems, it is noteworthy a recent paper by Liu et al. [151] that, by using MoO_3 and sulfur powder as solid precursors, have successfully synthesized by *in situ* CVD high-quality single-layer MoS_2 sheets on the atomically flat rutile TiO_2(110) single-crystal surfaces. The as-grown triangularly-shaped sheets on TiO_2 (110) single-crystal substrate are AFM imaged in Fig. 13 (upper panel). Notice from UV visible spectra (Fig. 13b, bottom panel on the left) the typical features of MoS_2 particles at the 650 nm and 605 nm due to the A and B excitonic peaks ([152] and ref. therein). The photoluminescence spectrum (PL) of the sample (Fig. 13c, bottom panel on the right), displayed a single highly symmetric peak centred at 652 nm corresponding to the aforementioned A excitonic emission of MoS_2, which is demonstrating the luminescing uniformity of the fabricated MoS_2 nanosheet.

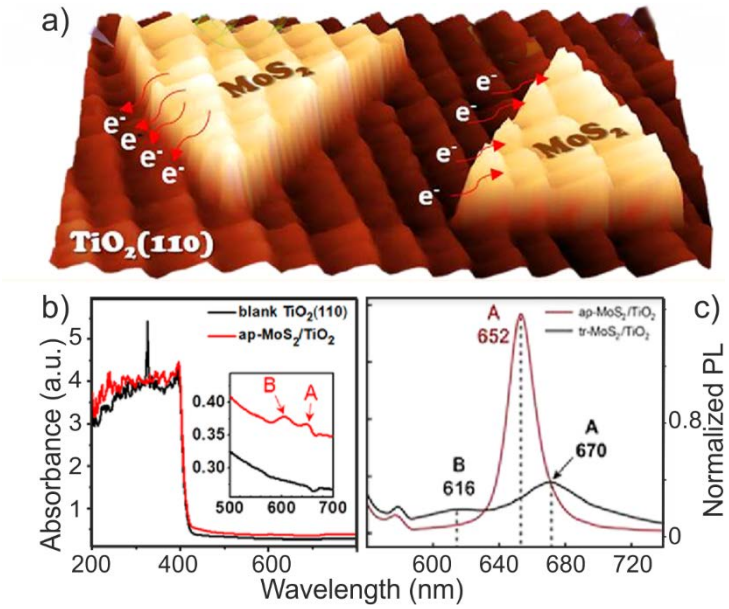

Fig. 13. a) 3D AFM image of single-layer MoS_2 sheets on TiO_2 (110) single-crystal substrate; b) UV-Vis spectrum of MoS_2/TiO_2 heterostructure (red line) as compared with rutile TiO_2 spectrum (black line); c) PL spectra of the same MoS_2/TiO_2 heterostructure as compared to 1L-MoS_2 transferred onto bare r-TiO_2 (110) surface. Reproduced with permission from ref. [151].

From the AFM, PL analyses and from other results, including STM, XPS, not reported for sake of brevity, the authors conclude that, beside the monolayer thickness, the single crystallinity of the MoS_2 adlayer as well as the atomic flatness of the composite surface, also the enhanced charge flow across the interface of MoS_2 /TiO_2 high quality heterojunctions under different irradiation conditions can be shown. Moreover, the authors state that the luminescence properties of MoS_2 are significantly tailored upon coupling with the TiO_2 surface. From all, it comes out that they have provided a proper TMD/oxide model system for a deeper understanding at the atomic level of the photocatalytic mechanisms occurring at the interface properties of the transition-metal dichalcogenides and oxide semiconductors.

In conclusion, in this section we stated the relevance of controlling the synthesis strategies to obtain high quality MoS_2 /TiO_2 heterostructures, thus highlighting the role of the interface, being the interface the 'heart' of the overall properties [62]. In summary we believe that, notwithstanding the huge amount of studies on the MoS_2 /TiO_2 based composites, to whose we remind the reader to refer, the research is still in an early stage and many challenges have to be addressed also to optimise synthesis methods and architectures of possible new advanced devices.

4. Summary and perspectives

In this review we focused on molecular and nanoscale phenomena occurring at TiO_2 surfaces as consequence of both the H_2O and CO_2 interaction or the grafting of organic/inorganic systems (graphene, MoS_2). More in detail, it is shown that the adsorption of water on TiO_2 surfaces is governed by a precise balance between molecular and dissociative adsorption, being the molecular adsorption favored on anatase (101) single crystals with a small coverage of water and the dissociative one on more defective higher energy surfaces, like those of the (110) type, as well as edges and corners. On these sites, it was found H_2O molecules to dissociate, forming hydroxy groups, which play an important role as scavenger of photogenerated holes, forming $^{\bullet}OH$ radicals. Some results are also reported on the activity of TiO_2 anatase nanoparticles with dominant (001) type facets, in comparison with "usual" TiO_2 anatase nanoparticles with a truncated bipyramidal shape, i.e. with dominant (101) type surface terminations. Some more, an important output of the interfacial water-TiO_2 events is the arising of superhydrophilicity of TiO_2 thin films by exposure to UV light. This phenomenon was recognized to have a relevant technological impact for the fabrication of photofunctional materials.

Concerning CO_2 interaction, from combined FTIR spectroscopy and periodic DFT calculations the role of the different surface sites in the CO_2 adsorption and reactivity on both dehydrated and hydrated TiO_2 anatase nanoparticles has been elucidated. It was stated that CO_2 is weakly adsorbed in molecular form at the most stable (101) surface, whereas the formation of carbonate and bicarbonate species is favoured at the (001) surface owing to the stronger (Lewis and Brønsted) basicity of its surface oxygens as well as on the low coordinated sites present on high index facets and on steps, edges and corners. These findings show that a controlled variation of the exposed anatase surfaces, exploiting shape-engineered nanoparticles can modify the reaction paths and improve the final CO_2 reduction performance. Lastly insights on the reaction pathways for the formation of carbon monoxide and methane from CO_2 photoreduction in presence of water vapor on oxygen-deficient anatase and brookite TiO_2 phases have been reported.

Moving to organic/inorganic hybrid materials, the acetylene/TiO_2 interaction has been shown as basis of a complex, but versatile, surface chemistry which can be addressed to the growth under mild conditions (like low temperature and low C_2H_2 pressure) and directly on the TiO_2 surface of a variety of meaningful products. These range from benzene and other small aromatic molecules, to strongly adsorbed coloured oligomeric chains up to graphene-like patches, or even continuous graphene layers, uniformly covering the oxide surface (*i.e.* organic surface structures possibly acting as stabilizers of the TiO_2 photo-charges. The progressive growth of products containing an increasing number of conjugated double bonds is consistent with the dramatic change in colour of the sample from white to intense blue, and with the contemporary formation of –O-H and saturated, hydrogen

rich, $–CH_3$ (and $–CH_2$) moieties, conjugated double bonds. These features have been fully explained with a concerted mechanism in which the extraction of hydrogen to form OH and methyl or alkyl groups is accompanied by self-assembling of the carbon-rich acetylene residues to form condensed products of high molecular weight. It has been shown that the reaction of acetylene with the TiO_2 surface in controlled conditions could represent a useful route for the *in-situ* preparation of uniform graphene layers at the surface of rutile TiO_2 single crystals and anatase TiO_2 nanosheets

Within the heterostructures grafted at the surface of TiO_2 polytypes, 2D layered materials such as MoS_2, has been discussed as promising material, also for its high activity, chemical stability, ability to modify the band gap from an indirect semiconductor (1.3 eV) to a direct semiconductor (1.9 eV), moving from the bulk to ultrathin and nanosized structures. Due to its favourable optical properties, that is, excitonic absorption bands in the visible and efficient interfacial charge-transfer region between MoS_2 and TiO_2 based materials, MoS_2 was considered of great interest to perform MoS_2/TiO_2 hybrid composites, made by TiO_2 sensitized with MoS_2, which causes to increase the visible light absorption ability of TiO_2-based systems. For this a few MoS_2/TiO_2-based heterostructures, obtained through different synthetic strategies, have been described, including *ex-situ* and *in-situ* approaches, by highlighting the main advantages and drawbacks of both approaches. Briefly from *ex-situ* methods highly heterogeneous MoS_2/TiO_2-based composites with weak interface interactions are often obtained, whereas from the *in-situ* methods, a more uniform dispersion of MoS_2/TiO_2-based composites has been shown. The peculiar role of the MoS_2/TiO_2 interface, in affecting the charge transport phenomena or the catalytic processes, which in turn are depending on the nature and atomic structure of the active sites, has been highlighted.

More in general we can state that by designing model systems of controlled morphology, the surfaces structure and then the specific reactivity of TiO_2 single crystal/nanoparticles or the interfaces structure of more complex MoS_2/TiO_2 based composites together the charge control phenomena can be properly tailored to the expected functionalities of the obtained architectures.

References.

1. A. Fujishima and K. Honda, Nature **238**, 37-38 (1972)
2. A. Tanaka, K. Teramura, S. Hosokawa, H. Kominami and T. Tanaka, Chem. Sci. **8**, 2574-2580 (2017)
3. M. Kitano, M. Matsuoka, T. Hosoda, M. Ueshima and M. Anpo, Res. Chem. Intermed. **34**, 577–585 (2008)
4. Y. Yoshida, M. Matsuoka, S.C. Moon, H. Mametsuka, E. Suzuki and M. Anpo, Res. Chem. Intermed. **26**, 567-574 (2000)
5. W.J. Feng, L.Y. Lin, H.J. Li, B. Chi, J. Pu and J. Li, Int. J. Hydrog. Energy **42**, 3938-3946 (2017)
6. S. Onsuratoom, S. Chavadej and T. Sreethawong, Int. J. Hydrog. Energy **36**, 5246-5261 (2011)
7. T.V. Nguyen, D.J. Choi and O.B. Yang, Res. Chem. Intermed. **31**, 483-491 (2005)
8. B. Abdollahi, A. Shakeri, S. Aber and M. Sharifi Bonab, Res. Chem. Intermed. **44**, 1505-1521 (2018)
9. Z. Boutamine, O. Hamdaoui and S. Merouani, Res. Chem. Intermed. **43**, 1709-1722 (2017)
10. L. Cermenati, A. Albini, P. Pichat and C. Guillard, Res. Chem. Intermed. **26**, 221-234 (2000)
11. D. Mas, P. Pichat and C. Guillard, Res. Chem. Intermed. **23**, 275-290 (1997)
12. L. Amalric, C. Guillard and P. Pichat, Res. Chem. Intermed. **21**, 33-46 (1995)
13. C. McCullagh, J.M.C. Robertson, D.W. Bahnemann and P.K.J. Robertson, Res. Chem. Intermed. **33**, 359-375 (2007)
14. A.A. Ashkarran, M. Ghavamipour, H. Hamidinezhad and H. Haddadi, Res. Chem. Intermed. **41**, 7299-7311 (2015)
15. R. Wang, K. Hashimoto, A. Fujishima, M. Chikuni, E. Kojima, A. Kitamura, M. Shimohigoshi and T. Watanabe, Nature **388**, 431-432 (1997)
16. A. Fujishima, K. Hashimoto and T. Watanabe, TiO2 Photocatalysis Fundamentals and Applications, (BKC Inc., Tokyo, 1999)
17. A. Fujishima, T.N. Rao and D.A. Tryk, J. Photochem. Photob. C Photochem. Rev. **1**, 1-21 (2000)
18. H. Nishikiori, M. Tagahara, L. Mukoyama and T. Fujii, Res. Chem. Intermed. **36**, 947-957 (2010)
19. S. Remiro-Buenamanana and H. Garcia, ChemCatChem **11**, 342-356 (2019)
20. W.G. Tu, Y. Zhou and Z.G. Zou, Adv. Mater. **26**, 4607-4626 (2014)

21. V. Jeyalakshmi, K. Rajalakshmi, R. Mahalakshmy, K.R. Krishnamurthy and B. Viswanathan, Res. Chem. Intermed. **39**, 2565-2602 (2013)
22. Y. Yamazaki, H. Takeda and O. Ishitani, J. Photochem. Photobiol. C-Photochem. Rev. **25**, 106-137 (2015)
23. B. Chen, Y. Meng, J. Sha, C. Zhong, W. Hu and N. Zhao, Nanoscale **10**, 34-68 (2018)
24. U. Diebold, Appl. Phys. A **76**, 681–687 (2003)
25. U. Diebold, Surf. Sci. Rep. **48**, 53-229 (2003)
26. X.-Q. Gong, A. Selloni, M. Batzill and U. Diebold, Nat. Mater. **5**, 665-670 (2006)
27. Y. Kubokawa and M. Anpo, Studies in Surface Science and Catalysis **21**, 127-138 (1985)
28. M. Anpo and M. Takeuchi, J. Catal. **216**, 505-516 (2003)
29. H.G. Yang, C.H. Sun, S.Z. Qiao, J. Zou, G. Liu, S.C. Smith, H.M. Cheng and G.Q. Lu, Nature **453**, 638-641 (2008)
30. A. Selloni, Nat. Mater. **7**, 613-615 (2008)
31. R. Asahi, T. Morikawa, T. Ohwaki, K. Aoki and Y. Taga, Science **293**, 269-271 (2001)
32. F. Cesano, D. Pellerej, D. Scarano, G. Ricchiardi and A. Zecchina, J. Photochem. Photob. a-Chem.

242, 51-58 (2012)
33. F. Cesano, I. Rattalino, F. Bardelli, A. Sanginario, A. Gianturco, A. Veca, C. Viazzi, P. Castelli, D. Scarano and A. Zecchina, Carbon **61**, 63-71 (2013)
34. E. Groppo, C. Lamberti, F. Cesano and A. Zecchina, PCCP **8**, 2453-2456 (2006)
35. H. Zangeneh, A.A.L. Zinatizadeh, M. Habibi and M.a. Akia, **26**, 1--36 (2015)
36. M.J. Uddin, D.E. Daramola, E. Velasquez, T.J. Dickens and J. Yan, Phys. Status Solidi RRL **8**, 898-903 (2014)
37. Y. Wang, S. Lkhamjav, B. Qiu, C. Dong, C. Dong, Y. Zhou, B. Shen, M. Xing and J. Zhang, Res. Chem. Intermed. **43**, 2055-2066 (2017)
38. M. Takeuchi, M. Matsuoka and M. Anpo, Res. Chem. Intermed. **38**, 1261-1277 (2012)
39. N. Sakaguchi Miyamoto, R. Miyamoto, E. Giamello, T. Kurisaki and H. Wakita, Res. Chem. Intermed. **44**, 4563-4575 (2018)
40. S.M. Chaudhari, P.M. Gawal, P.K. Sane, S.M. Sontakke and P.R. Nemade, Res. Chem. Intermed. **44**, 3115-3134 (2018)
41. J. Liu, L. Zhang, X. Yao and S.S.C. Chuang, Res. Chem. Intermed. **43**, 5041-5054 (2017)
42. S. Cravanzola, F. Cesano, F. Gaziano and D. Scarano, Catalysts **7**, 214 (2017)
43. B.P. Dhamaniya, A. Kumar, A.K. Srivastava and J.S. Tawale, Res. Chem. Intermed. **43**, 387-399 (2017)

44. Z. Youssef, L. Colombeau, N. Yesmurzayeva, F. Baros, R. Vanderesse, T. Hamieh, J. Toufaily, C. Frochot and T. Roques-Carmes, **159**, 49--71 (2018)

45. I.M. Kobasa, I.V. Kondratyeva, L.I. Odosiy and Y.V. Kropelnytska, Res. Chem. Intermed., 10.1007/s11164-019-03889-y, (2019)

46. A. Hagfeldt and M. Grätzel, Acc. Chem. Res. **33**, 269-277 (2000)

47. I. Robel, V. Subramanian, M. Kuno and P.V. Kamat, J. Am. Chem. Soc. **.128**, 2385-2393 (2006)

48. C. Sun, P. He, G. Pan, Y. Miao, T. Zhang and L. Zhang, Res. Chem. Intermed. **44**, 2607-2620 (2018)

49. B. Soman, S. Challagulla, S. Payra, S. Dinda and S. Roy, Res. Chem. Intermed. **44**, 2261-2273 (2018)

50. S. Bao, J. Wan, B. Tian and J. Zhang, Res. Chem. Intermed. **44**, 6137-6149 (2018)

51. C.Z. Wen, J.Z. Zhou, H.B. Jiang, Q.H. Hu, S.Z. Qiao and H.G. Yang, Chem. Commun. **47**, 4400-4402 (2011)

52. J. Yu, J. Lei, L. Wang, C. Guillard, J. Zhang, Y. Liu and M. Anpo, Res. Chem. Intermed., 10.1007/s11164-019-03903-3, (2019)

53. Y. Chen, Q. Dong, L. Wang, X. Guo, S. Ai and H. Ding, Res. Chem. Intermed. **44**, 7369-7389 (2018)

54. W. Zhang, Y. Zhou, C. Dong, B. Shen, M. Xing and J. Zhang, Res. Chem. Intermed. **44**, 4797-4807 (2018)

55. P. Verma and S.K. Samanta, Res. Chem. Intermed. **44**, 1963-1988 (2018)

56. J.C. Colmenares, R.S. Varma and P. Lisowski, **18**, 5736--5750 (2016)

57. B. Tang, H. Chen, H. Peng, Z. Wang and W. Huang, Nanomaterials **8**, 105 (2018)

58. K.R. Reddy, M. Hassan and V.G. Gomes, **489**, 1--16 (2015)

59. K. Lee, H. Yoon, C. Ahn, J. Park and S. Jeon, Nanoscale **11**, 7025--7040 (2019)

60. M. Baca, W. Kukuka, K. Cendrowski, E. Mijowska, R.J. Kaleczuk and B. Zieliska, **12**, 612--620 (2019)

61. S. Cravanzola, S.M. Jain, F. Cesano, A. Damin and D. Scarano, RSC Adv. **5**, 103255-103264 (2015)

62. B. Chen, Y. Meng, J. Sha, C. Zhong, W. Hu and N. Zhao, Nanoscale **10**, 34-68 (2018)

63. J. Shi, Chem. Rev. **113**, 2139--2181 (2013)

64. L.A. King, W. Zhao, M. Chhowalla, D.J. Riley and G. Eda, **1**, (2013)

65. W.K. Ho, J.C. Yu, J. Lin, J.G. Yu and P.S. Li, Langmuir **20**, 5865-5869 (2004)

66. T. Umeyama and H. Imahori, **46**, 15615-15627 (2017)

67. E. Singh and H.S. Nalwa, **7**, 1863-1912 (2015)

68. V. Etacheri, C. Di Valentin, J. Schneider, D. Bahnemann and S.C. Pillai, J. Photochem. Photob. C Photochem. Rev. **25**, 1-29 (2015)

69. I.A. Rusetskyi, M.O. Danilov, S.S. Fomanyuk, I.A. Slobodyanyuk, V.S. Vorobets and G.Y. Kolbasov, Res. Chem. Intermed., 10.1007/s11164-019-03895-0, (2019)

70. W. Iqbal, B. Tian, M. Anpo and J. Zhang, Res. Chem. Intermed. **43**, 5187-5201 (2017)

71. H.Y. He, J.H. Lin, W. Fu, X.L. Wang, H. Wang, Q.S. Zeng, Q. Gu, Y.M. Li, C. Yan, B.K. Tay, C. Xue, X. Hu, S.T. Pantelides, W. Zhou and Z. Liu, Adv. Energy Mater. **6**, (2016)

72. W.J. Han, C. Zang, Z.Y. Huang, H. Zhang, L. Ren, X. Qi and J.X. Zhong, Int. J. Hydrog. Energy **39**, 19502-19512 (2014)

73. B.A. Chen, E.Z. Liu, F. He, C.S. Shi, C.N. He, J.J. Li and N.Q. Zhao, Nano Energy **26**, 541-549 (2016)

74. B.A. Chen, E.Z. Liu, T.T. Cao, F. He, C.S. Shi, C.N. He, L.Y. Ma, Q.Y. Li, J.J. Li and N.Q. Zhao, Nano Energy **33**, 247-256 (2017)

75. S. Cravanzola, F. Cesano, F. Gaziano and D. Scarano, Front. Chem. **5**, 91 (91-12) (2017)

76. L. Guo, Z. Yang, K. Marcus, Z. Li, B. Luo, L. Zhou, X. Wang, Y. Du and Y. Yang, En. Environm. Sci. **11**, 106-114 (2018)

77. K.H. Hu, X.G. Hu, Y.F. Xu and X.Z. Pan, React. Kinet. Mech. Catal. **100**, 153-163 (2010)

78. Z. Yin, H. Li, H. Li, L. Jiang, Y. Shi, Y. Sun, G. Lu, Q. Zhang, X. Chen and H. Zhang, ACS Nano **6**, 74-80 (2012)

79. F. Cesano and D. Scarano, Coatings **8**, art. n. 419 (2018)

80. Y. Lin, P. Ren and C. Wei, CrystEngComm **21**, 3439–3450 (2019)

81. Y. Li, C. Cai, B. Sun and J. Chen, Semicond. Sci. Technol. **32**, art. n. 105011 (2017)

82. L. Zheng, S. Han, H. Liu, P. Yu and X. Fang, **12**, 1527-1536 (2016)

83. Y.J. Yuan, Z.J. Ye, H.W. Lu, B. Hu, Y.H. Li, D.Q. Chen, J.S. Zhong, Z.T. Yu and Z.G. Zou, **6**, 532-541 (2016)

84. S. Wang, B.Y. Guan, L. Yu and X.W.D. Lou, **29**, (2017)

85. W. Gao, M. Wang, C. Ran and L. Li, **51**, 1709-1712 (2015)

86. S. Cravanzola, L. Muscuso, F. Cesano, G. Agostini, A. Damin, D. Scarano and A. Zecchina, Langmuir **31**, 5469-5478 (2015)

87. R.D. Brown, R.A. Burton and P.M. Ku, ASLE Transactions **6**, 12-19 (1963)

88. T. Chinone and S. Okazaki, Nippon Kagaku Kaishi, 1327-1331 (1978)

89. Y. Nosaka, H. Sasaki, K. Norimatsu and H. Miyama, Chem. Phys. Lett. **105**, 456-458 (1984)

90. Y. Okamoto, A. Maezawa and T. Imanaka, J. Catal. **120**, 29-45 (1989)

91. J. Ramirez, S. Fuentes, G. Díaz, M. Vrinat, M. Breysse and M. Lacroix, Appl. Catal. **52**, 211-224 (1989)
92. K.C. Pratt, J.V. Sanders and V. Christov, J. Catal. **124**, 416-432 (1990)
93. Y. He, A. Tilocca, O. Dulub, A. Selloni and U. Diebold, Nat. Mater. **8**, 585-589 (2009)
94. G.S. Herman, Z. Dohnálek, N. Ruzycki and U. Diebold, J. Phys. Chem. B **107**, 2788-2795 (2003)
95. M. Setvin, B. Daniel, U. Aschauer, W. Hou, Y.-F. Li, M. Schmid, A. Selloni and U. Diebold, Phys. Chem. Chem. Phys., **16**, 21524-21530 (2014)
96. M. Primet, P. Pichat and M.V. Mathieu, J. Phys. Chem. **75**, 1216-1220 (1971)
97. A.A. Tsyganenko and V.N. Filimonov, J. Mol. Struct. **19**, 579-589 (1973)
98. C. Morterra, A. Chiorino, F. Boccuzzi and E.Z. Fisicaro, Phys. Chem. Neue Folge **124**, 211-222 (1982)
99. G. Busca, H. Saussey, O. Saur, J.C. Lavalley and V. Lorenzelli, Appl. Catal. **14**, 245-260 (1985)
100. K. Hadjiivanov, A. Davydov and D. Klissurski, Kinet. Katal. **29**, (1988)
101. C. Morterra, J. Chem. Soc., Faraday Trans. 1 **84**, 1617-1637 (1988)
102. K.I. Hadjiivanov and D.G. Klissurski, Chem Soc. Rev. **25**, 61-69 (1996)
103. S.H. Szczepankiewicz, A.J. Colussi and M.R. Hoffmann, J. Phys. Chem. B **104**, 9842-9850 (2000)
104. B. Erdem, R.A. Hunsicker, G.W. Simmons, E. David Sudol, V.L. Dimonie and M.S. El-Aasser, Langmuir **17**, 2664-2669 (2001)
105. K.S. Finnie, D.J. Cassidy, J.R. Bartlett and J.L. Woolfrey, Langmuir **17**, 816-820 (2001)
106. P. Du, A. Bueno-López, M. Verbaas, A.R. Almeida, M. Makkee, J.A. Moulijn and G. Mul, J. Catal. **260**, 75-80 (2008)
107. G. Martra, Appl. Cat. A Gen. **200**, 275-285 (2000)
108. X.Q. Gong, A. Selloni, M. Batzill and U. Diebold, Nat. Mater. **5**, 665-670 (2006)
109. L. Mino, G. Spoto, S. Bordiga and A. Zecchina, J. Phys. Chem. C **116**, 17008-17018 (2012)
110. C. Deiana, E. Fois, S. Coluccia and G. Martra, J. Phys. Chem. C **114**, 21531-21538 (2010)
111. C. Arrouvel, M. Digne, M. Breysse, H. Toulhoat and P. Raybaud, J. Catal. **222**, 152-166 (2004)
112. http://www.metecnetwork.eu/setnanometro-project/,
113. L. Mino, F. Pellegrino, S. Rades, J. Radnik, V.D. Hodoroaba, G. Spoto, V. Maurino and G. Martra, ACS Appl. Nano Mater. **1**, 5355-5365 (2018)

114. M. Takeuchi, L. Bertinetti, G. Martra, S. Coluccia and M. Anpo, Appl. Catal. A. Gen. **307**, 13-20 (2006)

115. M. Takeuchi, K. Sakamoto, G. Martra, S. Coluccia and M. Anpo, J. Phys. Chem. B **109**, 15422-15428 (2005)

116. L. Mino, G. Spoto and A.M. Ferrari, J. Phys. Chem. C **118**, 25016-25026 (2014)

117. Y.J. Cao, S.J. Hu, M. Yu, S.S. Yan and M.C. Xu, Phys. Chem. Chem. Phys., **17**, 23994-24000 (2015)

118. I. Kamber, Res. Chem. Intermed. **23**, 735-753 (1997)

119. A. Kubas, D. Berger, H. Oberhofer, D. Maganas, K. Reuter and F. Neese, J. Phys. Chem. Lett. **7**, 4207-4212 (2016)

120. Y.J. Cao, M. Yu, S.D. Qi, T.T. Wang, S.M. Huang, Z.F. Ren, S.S. Yan, S.J. Hu and M.C. Xu, Phys. Chem. Chem. Phys., **19**, 31267-31273 (2017)

121. L.F. Liao, C.F. Lien, D.L. Shieh, M.T. Chen and J.L. Lin, J. Phys. Chem. B **106**, 11240-11245 (2002)

122. J. Baltrusaitis, J. Schuttlefield, E. Zeitler and V.H. Grassian, Chem. Eng. J. **170**, 471-481 (2011)

123. L. Mino, G. Spoto, S. Bordiga and A. Zecchina, J. Phys. Chem. C **117**, 11186-11196 (2013)

124. F. Pellegrino, F. Sordello, L. Mino, C. Minero, V.D. Hodoroaba, G. Martra and V. Maurino, ACS Catal., 10.1021/acscatal.9b01861, 6692-6697 (2019)

125. Z. Xiong, Z. Lei, Y.Z. Li, L.C. Dong, Y.C. Zhao and J.Y. Zhang, J. Photochem. Photobiol. C-Photochem. Rev. **36**, 24-47 (2018)

126. L.J. Liu, H.L. Zhao, J.M. Andino and Y. Li, ACS Catal. **2**, 1817-1828 (2012)

127. L.J. Liu, F. Gao, H.L. Zhao and Y. Li, Appl. Catal. B-Environ. **134**, 349-358 (2013)

128. Y. Wang, J. Zhao, T.F. Wang, Y.X. Li, X.Y. Li, J. Yin and C.Y. Wang, J. Catal. **337**, 293-302 (2016)

129. L.J. Liu, C.Y. Zhao, J.T. Miller and Y. Li, J. Phys. Chem. C **121**, 490-499 (2017)

130. M. Anpo, S.C. Moon, K. Chiba, G. Martra and S. Coluccia, Res. Chem. Intermed. **19**, 495-519 (1993)

131. A. Zecchina, D. Scarano, S. Bordiga, G. Spoto and C. Lamberti, Surface structures of oxides and halides and their relationships to catalytic properties, (Academic Press Inc, 2001)

132. J.C. Védrine, Res. Chem. Intermed. **41**, 9387-9423 (2015)

133. A.V. Ivanov, A.E. Koklin, E.B. Uvarova and L.M. Kustov, PCCP **5**, (2003)

134. K.G. Pierce and M.A. Barteau, **98**, 3882--3892 (1994)

135. A.B. Sherrill and M.A. Barteau, **184**, 301--310 (2002)

136. A.H. Boonstra and C.A.H.A. Mutsaers, J. Phys. Chem. **79**, 2025-2027 (1975)

137. V. Rives-Arnau and N. Sheppard, **76**, 394--402 (1980)

138. V. Rives-Arnau and N. Sheppard, **77**, 953--961 (1981)

139. S.M. Jain, J.J. Biedrzycki, V. Maurino, A. Zecchina, L. Mino and G. Spoto, J. Mater. Chem. A **2**, 12247-12254 (2014)

140. J.J. Biedrzycki, S. Livraghi, I. Corazzari, L. Mino, G. Spoto and E. Giamello, Langmuir **31**, 569-577 (2015)

141. H.Y.T. Chen, S. Livraghi, E. Giamello and G. Pacchioni, **81**, 64--72 (2016)

142. H. Liu, Z. Chen, L. Zhang, D. Zhu, Q. Zhang, Y. Luo and X. Shao, **122**, 6388--6396 (2018)

143. H. Liu, D. Zhu, H. Shi and X. Shao, ACS Omega **1**, 168-176 (2016)

144. S. Cravanzola, M. Sarro, F. Cesano, P. Calza and D. Scarano, Nanomaterials **8**, 207(201-215) (2018)

145. J. Jun Zhang, L. Zhang, X. Ma and Z. Ji, Appl. Surf. Sci. **430**, 424-437 (2018)

146. X. Zhu, C. Yang, F. Xiao, J. Wang and X. Su, New J. Chem. **39**, 683-688 (2015)

147. D. Scarano, F. Cesano and A. Zecchina, J. Phys. Chem. C **123**, 7799-7809 (2019)

148. W.D. Schneider, M. Heyde and H.J. Freund, Chem. Eur. J. **24**, 2317–2327 (2018)

149. H. Wang, D. Kong, P. Johanes, J.J. Cha, G. Zheng, K. Yan, N. Liu and Y. Cui, Nano Lett. **13**, 3426-3433 (2013)

150. F. Cesano, S. Bertarione, A. Piovano, M.M. Rahman, G. Agostini, E. Groppo, F. Bonino, C. Lamberti, D. Scarano, S. Bordiga, L. Montanari, L. Bonoldi, R. Millini and A. Zecchina, Catal. Sci. Technol. **1**, 123-136 (2011)

151. H. Liu, Y. Li, M. Xiang, H. Zeng and X. Shao, ACS Nano **13**, 6083-6089 (2019)

152. S. Cravanzola, F. Cesano, G. Magnacca, A. Zecchina and D. Scarano, RSC Adv. **6**, 59001-59008 (2016)